Pressure Induced Electronic Topological Transition from Band to Topological Insulator in Sb_2Se_3

A Thesis

Submitted in partial fulfillment for the Degree of

Master of Science

as a part of Integrated Ph.D. programme in

Materials Science

by

Koushik Pal

Chemistry and Physics of Materials Unit
Jawaharlal Nehru Centre for Advanced Scientific Research
Bangalore – 560 064

MARCH 2013

To my parents

DECLARATION

I hereby declare that the matter embodied in the thesis entitled " **Pressure Induced Electronic Topological Transition from Band to Topological Insulator in Sb_2Se_3**" is the result of investigations carried out by me at the Chemistry and Physics of Materials Unit, Jawaharlal Nehru Centre for Advanced Scientific Research, Bangalore, India under the supervision of Prof. Umesh V. Waghmare and that it has not been submitted elsewhere for the award of any degree or diploma.

In keeping with the general practice in reporting scientific observations, due acknowledgement has been made whenever the work described is based on the findings of other investigators.

Koushik Pal

CERTIFICATE

I hereby certify that the matter embodied in this thesis entitled " **Pressure Induced Electronic Topological Transition from Band to Topological Insulator in Sb_2Se_3**" has been carried out by Mr. Koushik Pal at the Chemistry and Physics of Materials Unit, Jawaharlal Nehru Centre for Advanced Scientific Research, Bangalore, India under my supervision and that it has not been submitted elsewhere for the award of any degree or diploma.

Prof. Umesh V. Waghmare
(Research Supervisor)

Acknowledgements

First of all I want to thank my supervisor Prof. Umesh V. Waghmare for his constant guidance and motivation all through the research work. The work which I have done, would not be possible without his help and advices. He always provides me enormous amount of freedom in workplace. His enthusiasm and zeal towards scientific research inspire me a lot. It's always been a great pleasure and opportunity for me to work with him.

I am very grateful to all the members of the Materials Theory Group who helped me in many ways during this project and in fact I have learned a lot from seniors like Dr. Abhishek, Sharmila, Jayashree, Summayya. I am also very thankful to other members of the group Vinay, Anjali, Meha, Suchitra and Aysha.

The life outside the lab was made enjoyable by the good presence of my Integrated Ph.D. batch-mates Anirban, Ankush, Arkamita, Chandan(s), Ram, Rajasekhar and Sisir. I have been benefitted a lot from them during the coursework as well as during my leisure time. I also owe a lot to the senior Ph.D. and Integrated Ph.D. students whose help (or advices) made both my academic and non-academic life a memorable and a comfortable one here at JNC.

I am highly indebted to Prof. S. Balasubramanian, Prof. A. Sundaresan, Prof. S. M. Shivaprasad, Prof. C. Narayana, Prof. K. S. Narayan, Prof. G. U. Kulkarni, Dr. R. Ganapathy, Dr. R. Datta, Prof. T. K. Maji, Prof. M. Eswaramoorthy, Prof. S. Narasimhan, Prof. U. V. Waghmare, Prof. Subir K. Das and Prof. A. Chakraborty (IISc) whose classes during the course-work greatly helped me in my research. Being very nice to the students, it's always been a great pleasure to discuss with them about any scientific and non-scientific issues.

I want to thank our collaborators Prof. A. K. Sood and his student Achintya from the Dept. of Physics, IISc. I have learned a lot whenever we had any meeting or discussion with them. I am highly motivated by their way of understanding or questioning any subject in a deeper level.

I convey deepest respect to those teachers in my village who always inspired and motivated me to pursue higher studies. My sincere thanks also go to my childhood friends with whom I spent the first best fifteen years of my life.

Finally, it will be an incomplete task if I forget to acknowledge my parents. It's their unconditional love and support which help me accomplishing my dream. Last but not least, I want to thank my brother Anirban for always standing by me in all situations.

Synopsis

Density functional theory (DFT) has played significant role in predicting and explaining novel functional materials and properties in chemistry, materials science as well as in condensed matter physics in the last few decades. DFT has been used to shed light on problems which is hard and expensive to accomplish experimentally.

In the recent years discovery of a new class of exotic materials known as Topological insulator (TI) has led to the discovery of very interesting quantum states of matter like robust surface states, anomalous Hall effect, Majorana fermion etc. Hence these materials are good candidates not only for research but also for many practical applications like quantum computation. So far, only few TI have been discovered and realized, therefore it's necessary to find new materials which has topologically protected non-trivial states of matter. In my research, I have extensively used DFT to find so-called TI materials. With the help of state-of-the-art *ab-initio* calculations and theoretical model based analysis, we have been able to show that Sb_2Se_3 which is a band insulator, can be transformed into topological insulator by applying pressure on the single crystal of Sb_2Se_3.

My thesis is divided into three chapters. In the first chapter I have discussed

the importance of total energy calculations with a brief introduction to band and topological insulators, topological invariants, consequences of relativistic effects in solids and electron-phonon coupling. Theoretical background of the method used to study the material is given concisely in the second chapter. The third chapter includes pressure dependent investigations and results of Sb_2Se_3 along with dynamical corrections to phonon frequencies which require analysis beyond adiabatic *Born-Oppenheimer* approximation. Group theoretical techniques have been discussed in appendices.

List of Publications

1. "Sharp Raman Anomalies and Broken Adiabaticity at a Pressure Induced Transition from Band to Topological Insulator in Sb_2Se_3", Achintya Bera, **Koushik Pal**, D. V. S. Muthu, Somaditya Sen, Prasenjit Guptasarma, Umesh V. Waghmare and Ajay K. Sood, Phys. Rev. Lett. **110**, 107401 (2013).
   (Invited and to be published as "Research Highlights" in the fourth issue of the "Asia Pacific Physics Newsletter", May 2013.)

2. "Pressure Dependent Investigations of Binary Semiconductors Bi_2Se_3 and Sb_2Se_3: A Detailed First-principles Study", **Koushik Pal** and Umesh V. Waghmare, (Manuscript under preparation).

List of Figures

List of Tables

Contents

Chapter 1

Introduction

1.1 Total energy calculation

Every material consists of electrons and ions. Microscopic investigations of various macroscopic properties of a material reveal that most of the properties arise due to the interaction between the electrons and the ions and the interaction among themselves. The behavior of these atomic and subatomic particles can best be described by quantum theory very accurately. This revolutionary theory, which evolved in the beginning of the twentieth century to explain the hidden nature of an atom, was successfully applied to many problems in physics. The most successful example being the explanation of fine structure splitting of the spectral lines of H atom. With the help of quantum theory, the experimental results for the fine structure constant was reproduced very accurately [1]. The success of quantum theory leads scientist to apply it in solid state physics to explain and predict various physical properties of a material.

Nearly all physical properties of materials are related to total energies or difference between total energies [2–5]of the electrons and ions. For example equilibrium lattice constant of a material is the lattice constant at which total energy is minimum, the spring constant of a material is related to second derivative of total energy with respect to atomic displacement. From the elastic constant we can calculate the phonon frequencies. Total energy techniques have also been used successfully to predict dielectric constant, piezo-electric constant, Born dynamical charges, magnetic susceptibility and many more physically measurable quantities of materials. To get the total energy of a system containing electrons and ions, we need to solve the Schrödinger equation. But solving the Schrödinger equation is not very easy as electrons interact with the ions via electromagnetic field and hence electronic degrees of freedom are coupled to ionic degrees of freedom which give rise to a coupled differential equation. On the other hand, as the system becomes complex containing many electrons and ions, solving the Schrödinger equation become practically impossible. To get rid of these difficulties, we need good approximations, new theoretical algorithms and powerful computers. In literature, there exist many methods to calculate the total energy of a system like *Hartree-Fock* method, *orthogonalized plane wave* (OPW) method, *augmented plane wave* (APW) technique, tight binding or *linear combination of atomic orbital* (LCAO) method etc. But among all these methods, pseudopotential theory based *density functional theoretical* (DFT) calculation turns out to be most widely used in the scientific community. It simplifies the computation of total energy even for a complex system containing few hundreds to thousand atoms to a great extent. We call this method

ab-initio because it requires only the specification of atomic number and no other parameters. This thesis contains several applications of *ab-initio* density functional theory.

1.2 Insulators

One of the most fascinating states of matter, which is known to mankind almost over two centuries, is the insulating state of material. According to the mean field description of band theory [6–8], insulators are characterized by a gap in the single particle energy spectrum of the periodic Hamiltonian of a solid where the Fermi level lies in the gapped region and as a consequence it has zero conductivity when the temperature approaches absolute zero temperature. If the Fermi level lies elsewhere instead of the gap and crosses any band, then it is said to be a metal. The linear response of a system in an external electric field also identifies insulator from that of the metals. If the electric field induces an electric polarization in the system without any conduction of current, then the system is said to an insulator. The modern classification of any insulators, inspired from the historic work by W. Kohn [9] who discriminates insulators from metal with their non-overlapping localized wave functions (very similar to localized Wannier function) in many-particle configuration space, are based on the geometrical properties (Berry phase, Berry curvature, Chern number etc.) of the many-body wave function. The geometrical features of a wave function also allow us to define macroscopic properties of such systems. As an example, according to the modern theory of polarization, Berry phase is crucial in determining the macroscopic

polarizability of an insulator [10–12]. It is the geometric phase of the wave functions which distinguish band insulator, Mott insulator, Anderson insulator, Chern insulator and Topological insulator from each other [13]. Here I will provide a short description of topological insulator which is the prime topic of this thesis.

1.2.1 Topological insulator

Topological insulator is a novel quantum state of matter in the sense that the interior of the material has a bulk band gap behaving perfectly like an insulator but having metallic properties in its surface. Until the late twentieth century every phase in condensed matter physics was classified to be associated with a spontaneous broken symmetry of the system, but the discovery of quantum spin Hall effect [14–16] embark on a different classification based on the topological order of the material. Quantum spin Hall effect arises in certain materials like $HgTe$ quantum wells even in the absence of any magnetic field with symmetry protected topological state [17]. Topological insulator is a kind of exotic material which has distinct ordered topological state without any spontaneous broken symmetry. Theoretical model based analysis and electronic structure calculations on the surface of a topological insulator reveal that electronic bands of the surface states are spin polarized and they form Dirac cones in the time reversal invariant momenta (TRIM) points in the Brillouin zone which reside within the bulk gap of that material. Topological insulators are classified as strong or weak depending on whether they have odd and even number of Dirac cones on the surface respectively. The

surface states, which are protected by strong spin-orbit coupling by virtue of Kramer's theorem from any time-reversal invariant perturbation, possesses chiral spin textures. Because of this helical spin textures at the edge states, the spin of the electron is locked with its momentum and thus it is different from conventional quantum Hall insulators. This spin-momentum locking behavior paves the way to host Majorana fermion, an elusive quasi-particle which is their own anti-particle, on the surface of a topological insulator if it is proximity-coupled to a bulk superconductor [18, 19]. Majorana fermions follow neither fermionic statistics nor bosonic statistics, instead it obeys non-abelian quantum statistics and so it can be used for many practical purposes like fault tolerant conduction of current [20]. As the behavior of the electronic charge carriers on the surface of a topological insulator is described by relativistic Dirac equation, they are often called as Dirac fermion which are massless and obey relativistic principles. Due to this massless-ness, electronic dispersion relation becomes linear and hence when the top of the valence band and bottom of the conduction band touch with each other to give rise to metallic state on the surface, it forms a cone which is known as Dirac cone. Inclusion of relativistic effect in electrons ensures the nature of strong spin-orbit coupling in topological insulators which play a major role in topological phase transition in these materials. A guiding principle to search for topological insulator would be to find a material where top of valence and bottom of conduction bands have opposite parities and the inversion of those bands occur with respect to any internal or external parameters e.g. spin-orbit coupling, dc electric field [21], stoichiometry of a compound [22],

pressure [23], electron-phonon coupling [24] etc.. In centro-symmetric material the quantum phase transition between topological trivial phase and topological non-trivial phase occurs when the sign of the Dirac fermions' mass get inverted at the TRIM points in the bulk Brillouin zone.
Since topological insulator possesses single particle energy gap in the bulk and electron-electron interaction does not effect the energy states in an essential way, single particle quantum mechanical approach can be used to describe the electrons in a topological insulator and thus can be treated within the band theory of solid. It is this reason which allow us to treat topological insulator within the framework of density functional theory (DFT). In the second chapter we will see the technical details of DFT calculations.

1.2.2 Topological invariants

The main purpose of topology in mathematics is to classify spaces. For example, 2D surfaces can be topologically classified by the number of holes in them. Mathematically, the quantity which is used to classify 2-D surfaces, is related to the genus g of that surface. For instance, a sphere and a donut are classified by $g = 0$, and $g = 1$ respectively. In topology, we consider two objects to be topological invariant if they can be transformed into another by a smooth continuous deformation. Quantifying the topological invariant quantity mathematically is not very easy but in two-dimensional cases, the problem is greatly simplified by *Gauss-Bonnet* theorem which states that the integral of the Gaussian curvature over a closed surface is a quantized topological invariant and is related to g as defined earlier.

3D topological insulators belong to $\mathbb{Z}_2$ invariant class [25] which is characterized by the second Chern number. The Chern number of a topological insulator can be defined as the total Berry flux associated with the Berry phases acquired by the Blöch wave function $u_m(\mathbf{k})$, when $\mathbf{k}$ is transported across a closed loop in the Brillouin zone [26]. So clearly topological invariant is related to the geometry or topology of the object under study, here it is the insulator and hence the name topological insulator is justified.

Unlike Hall insulators, the topological non-trivial state exists even in the presence of time reversal symmetry, which is due to spin-orbit coupling in the system [26]. All the eigenstates of a time reversal invariant insulators are at least two-fold degenerate which is a consequence of Kramer's theorem. In the absence of spin-orbit coupling up spins and down spins form Kramer's degenerate pair. But in the presence of spin-orbit coupling, however, it has non-trivial consequences. The Hamiltonian of a time reversal invariant insulator must satisfy $\Theta\mathcal{H}(\mathbf{k})\Theta^{-1} = \mathcal{H}(\mathbf{-k})$, where Θ is the time reversal operator. The second Chern number of a topological insulator remains invariant under any continuous deformation of $\mathcal{H}$ as long as no level crossing occurs at Fermi level.

Topological insulators can further be divided into two classes strong topological insulator and weak topological insulator based on the values of four $\mathbb{Z}_2$ topological invariants $(\nu_0; \nu_1\nu_2\nu_3)$. Those four invariants can be understood by bulk-boundary correspondence. The surface Brillouin zone of a 3D topological insulator contains four TRIM points- $\Gamma_{1,2,3,4}$ [27, 28]. The surface states are degenerate owing to Kramer's theorem at those special points in the Brillouin zone, but away from these points, the degeneracy of surface

states are lifted by spin-orbit coupling. Now depending upon how the surface states connect with each other between any pair of $\Gamma_{1,2,3,4}$ points, we will define strong and weak classification of topological insulators. If the surface states cross even number of time, then the metallic surface state is not protected under any disorder or time reversal invariant perturbation. We call this type of insulators as weak topological insulator. On the other hand for strong topological insulator the surface states connect the Fermi level odd number of time and the metallic state is protected under any time reversal invariant perturbation and strong disorder. Since time reversal symmetry requires electronic wave functions with **k** and **-k** have opposite spins, the spins must rotate with **k** in the Fermi surface giving rise to a helical spin orientation (see Fig. 1.1).

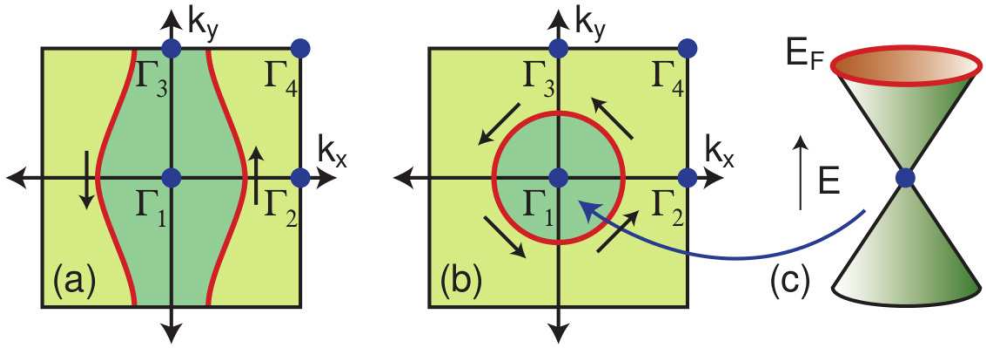

Figure 1.1: *Fermi circles in the surface Brillouin zone for (a) a weak topological insulator and (b) a strong topological insulator. In the simplest type of strong topological insulator, the Fermi circle encloses a single Dirac point. (c) Kramer's degeneracy at the TRIM points in the Brillouin zone. This figure has been taken from M. Z. Hasan and C. L. Kane, Rev. Mod. Phys.* ***82****, 3045 (2010). "Copyright (2010) by the American Physical Society."*

This helical arrangements of spins help the electrons to acquire a non-trivial Berry's phase of 0 or π. The π Berry's phase leads to weak anti-localization [29] in a strong topological insulator due to the destructive interference of the backscattered electrons from any disorder in the system as long as the bulk energy gap remains finite and intact [30].

1.3 Relativistic effects in solid

According to the (special) theory of relativity, the mass of an object varies as $m = \frac{m_0}{\sqrt{1-(v^2/c^2)}}$, where v is the velocity of the electrons and c is the speed of light in vacuum. Now if the velocity of the electrons becomes comparable to that of the speed of light, then mass of the electron increases and radius of an electron orbital which is inversely proportional to its mass, shrinks compared to what it would have been without the relativistic effect. The relativistic effect is more pronounced for the inner orbitals of an atom. As a result, the screening effect on the outer orbitals become more stronger and the energy of the outer shells go up. This may have severe consequences on various properties of a solid, for example, in the bond lengths, spectroscopic properties (Lamb shift) etc. As a practical example, in Hg atom, the orbital radius of $1S$-shell electrons, whose $v/c = 0.58$, shrink by 23% [31]. From elementary quantum mechanics we know that, velocity of an electron is proportional to Z (atomic number) of an atom. So, the relativistic effect becomes more prominent for heavy elements. Another important aspect of relativistic effect is the spin-orbit coupling which has very significant role in molecules (e.g. fine structure splitting of spectral lines in H atom) and solids (e.g. lattice

parameter [32] and optical properties [33] of gold) especially in topological insulators. Important aspect of spin-orbit coupling on topological insulator will be discussed later in this thesis. Now we will discuss about spin-orbit coupling.

One of the greatest triumphs of the twentieth century science is to successfully combine special theory relativity and quantum mechanics to unravel many hidden mysteries in physics. After the initial efforts of Gordon & Klein, it was the British physicist P. A. M. Dirac who was able to give a successful and elegant theory of relativistic quantum mechanics. The Dirac Hamiltonian for a free particle is given by,

$$H = c\boldsymbol{\alpha}.\mathbf{p} + \beta mc^2, \tag{1.1}$$

where $\mathbf{p} = -i\hbar\nabla$ is the momentum operator and c is the speed of light in vacuum. It can be shown that, to get the solution of the Dirac Hamiltonian, minimum order of $\boldsymbol{\alpha}$ and β would be four [34]. Among the infinite number of possible solutions, the standard form of $\boldsymbol{\alpha}$ and β are give below.

$$\boldsymbol{\alpha} = \begin{pmatrix} 0 & \boldsymbol{\sigma} \\ \boldsymbol{\sigma} & 0 \end{pmatrix} \qquad \beta = \begin{pmatrix} I_{2\times2} & 0 \\ 0 & -I_{2\times2} \end{pmatrix} \tag{1.2}$$

Where $\boldsymbol{\sigma}$ is the Pauli spin matrices. Three component of Pauli spin matrices $\boldsymbol{\sigma}$ are given by,

$$\boldsymbol{\sigma}_1 = \begin{pmatrix} 0 & 1 \\ 1 & 0 \end{pmatrix} \qquad \boldsymbol{\sigma}_2 = \begin{pmatrix} 0 & -i \\ i & 0 \end{pmatrix} \qquad \boldsymbol{\sigma}_3 = \begin{pmatrix} 1 & 0 \\ 0 & -1 \end{pmatrix} \tag{1.3}$$

$I_{2\times2}$ is a unit matrix of order 2.

The Dirac Hamiltonian for a charged particle q in the presence of an electromagnetic field $(\mathbf{A}, \phi)$ can be written as [35],

$$H = c\boldsymbol{\alpha}.(\mathbf{p} - q\mathbf{A}) + q\phi + \beta mc^2, \tag{1.4}$$

where $\mathbf{A}$ is the magnetic vector potential and ϕ is the scalar electrostatic potential. Eq. (1.4) can be put into the form as,

$$[(E - q\phi) - c\boldsymbol{\alpha}.(\mathbf{p} - q\mathbf{A}) - \beta mc^2]\psi(\mathbf{r}) = 0, \tag{1.5}$$

where $\psi(\mathbf{r})$ is the four component spinor wave function for the Dirac equation. The four component spinor wave function can be written in terms two component function $\phi(\mathbf{r})$ and $\eta(\mathbf{r})$ as follows,

$$\psi(\mathbf{r}) = \begin{pmatrix} \phi(\mathbf{r}) \\ \eta(\mathbf{r}) \end{pmatrix} \tag{1.6}$$

For central field (Coulomb potential near the nucleus) $\mathbf{A} = 0$ and $q\phi = -e\phi = V(\mathbf{r})$. In terms of two component functions using Eq. (1.6) in Eq. (1.5), we have,

$$\begin{aligned} E\phi(\mathbf{r}) &= c(-i\hbar\boldsymbol{\nabla} - q\mathbf{A}).\boldsymbol{\sigma}\eta(\mathbf{r}) + (q\phi + mc^2)\phi(\mathbf{r}) \\ E\eta(\mathbf{r}) &= c(-i\hbar\boldsymbol{\nabla} - q\mathbf{A}).\boldsymbol{\sigma}\phi(\mathbf{r}) + (q\phi - mc^2)\eta(\mathbf{r}) \end{aligned} \tag{1.7}$$

So, in a Coulomb field of a nucleus and in the non-relativistic limit of the Dirac equation, from Eq. (1.7), we can write,

$$\eta(\mathbf{r}) = \frac{1}{E' + 2mc^2 - V(r)} c(-i\hbar\boldsymbol{\sigma}.\boldsymbol{\nabla})\phi(\mathbf{r}), \tag{1.8}$$

where $E = E' + mc^2$. This is written to separate the non-relativistic contribution in Dirac equation. $|E'|$ and $|q\phi|$ are much smaller than mc^2 term. Substituting Eq. (1.8) in the first equation of Eq. (1.7) and expanding $[E' + 2mc^2 - V(r)]^{-1}$ to lowest order we get,

$$\begin{aligned} E'\phi(\mathbf{r}) = \Bigg[&- \frac{\hbar^2}{2m}\boldsymbol{\nabla}^2 + V(r) + \frac{\hbar^2}{2m}\frac{E' - V(r)}{2mc^2}\boldsymbol{\nabla}^2 + \frac{1}{2m^2c^2}\frac{1}{r}\frac{dV}{dr}\mathbf{L}.\mathbf{S} \\ &- \frac{\hbar^2}{4m^2c^2}\frac{dV}{dr}\frac{\partial}{\partial r}\Bigg]\phi(\mathbf{r}) \end{aligned} \tag{1.9}$$

where the third term represent the spin-orbit coupling, denoted as H_{SO}.

$$H_{SO} = \frac{1}{2m^2c^2}\frac{1}{r}\frac{dV}{dr}\mathbf{L}.\mathbf{S}. \tag{1.10}$$

While arriving at Eq. (1.9), we have used the following relations,

$$\begin{cases} [E' + 2mc^2 - V(r)]^{-1} \simeq \frac{1}{2mc^2}[1 - \frac{E' - V(\mathbf{r})}{2mc^2}] \\ \mathbf{L} = \mathbf{r} \times \mathbf{p} = \mathbf{r} \times (-i\hbar\boldsymbol{\nabla}) \\ \mathbf{S} = i\hbar\boldsymbol{\sigma}/2 \end{cases} \tag{1.11}$$

Here $\mathbf{L}$ and $\mathbf{S}$ represent total orbital angular momentum and spin angular momentum of an atom respectively. So, we see that the spin-orbit interaction is captured automatically in relativistic quantum mechanics through the Dirac's equation. Physically the origin of spin-orbit coupling can be described as follows. Being a charged particle, an electron in an atom sees a magnetic field because of its own orbital motion. Apart from that, it has intrinsic spin magnetic moment. Interaction between these two magnetic contributions give rise to spin-orbit coupling. The effect of spin-orbit interaction is to split the atomic energy levels and the degeneracy in energy bands in solids. As an example the spin-orbit interaction lifts the degeneracy of the electronic structure in topological insulator like Bi_2Se_3 in any k-point in the Brillouin zone other than the four TRIM points where degeneracy is preserved owing to Kramer's theorem. A schematic diagram for effect of spin-orbit interaction on the energy band of topological insulator is shown in Fig. 1.2. The magnitude of spin-orbit interaction is roughly proportional to Z^3 or Z^4. The physical reasoning behind this is that, as Z increases the number of electrons also increase, thereby the electron experience more and more stronger internal magnetic field. Hence the interaction energy also becomes larger. In crystalline solids the spin-orbit interaction is $\mathbf{k}$-dependent. For example in

cubic materials, at L-point in the Brillouin zone the spin-orbit splittings are typically 2/3 order of magnitude smaller than at Γ-point [36].

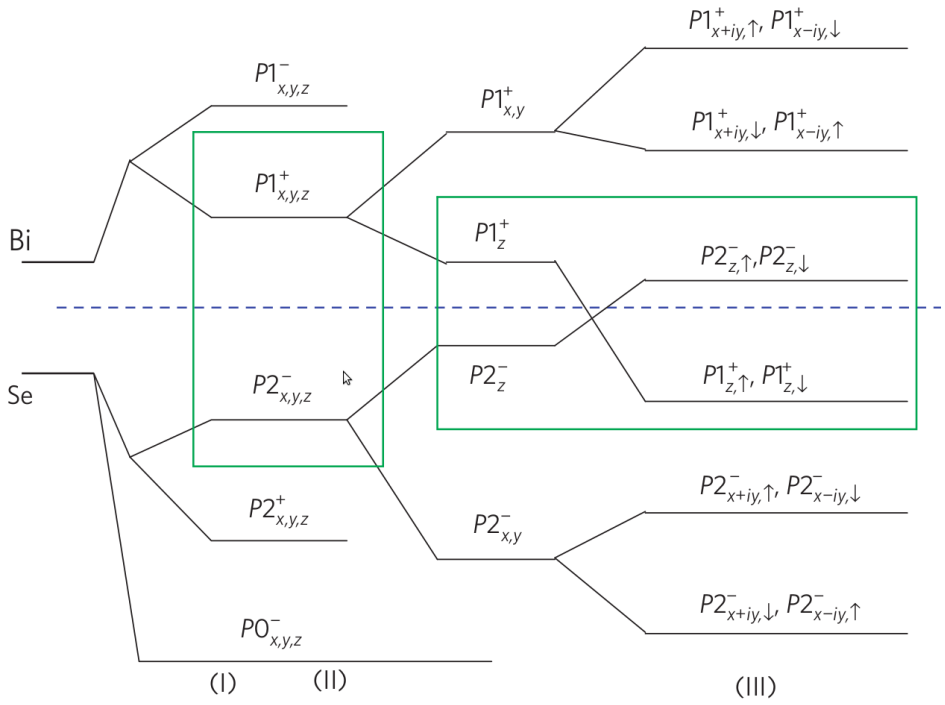

Figure 1.2: *Schematic band diagram of the evolution from the atomic $p_{x,y,z}$ orbitals of Bi and Se into the conduction and valence bands of Bi_2Se_3 at the Γ point. The three different stages (I), (II) and (III) represent the effect of tuning on chemical bonding, crystal field splitting and SOC respectively. The blue dashed line represents the Fermi energy. This figure has been taken from H. Zhang, C. X. Liu, X. L. Qi, X. Dai, Z. Fang and S. C. Zhang, Nature Physics **5**, 438 (2009). "Copyright (2009) by the American Physical Society".*

1.4 Electron-phonon interaction

At finite temperature every material has spontaneous vibration of its constituent ions, regardless of how small it becomes. The quantization of lattice

vibration is called phonon. When a phonon disturbs a lattice by moving some atoms away from its equilibrium sites, the electrons also change their positions. Thus the electrons are liable to be deflected or scattered. The local deformation in the lattice caused by the phonons or the vibration of ions change the effective electrostatic potential acting on the electrons and thereby creates a possibility of the electrons to be scattered from their usual course. This phenomenon where the change in effective potential force the electron to interact with the lattice vibration is called electron-phonon interaction. Like in the case of phonon-phonon scattering, the principle of conservation of wave vectors is also obeyed in electron-phonon interaction and whenever an electron is scattered, a phonon must be absorbed or emitted.

When an atom moves in crystal due to lattice vibrations, it does not carry with it all the electrons. Instead, the ions move through the background of an electron gas which is made up of the wave functions of all the electrons extending all over the crystal. This electron gas is not static but capable of collective motion to shield out any variation in electrostatic potential caused by the ionic motion. In the long wavelength limit, when the phonon wave vector is much greater than the screening length of the electrons, we can separate out the electronic motion from that of the ionic part in the total Hamiltonian of the system. This approximation is often called as adiabatic *Born-Oppenheimer* approximation. The total Hamiltonian of a system can be written as,

$$\mathcal{H} = \sum_I \frac{\mathbf{P}_I^2}{2M_I} + V(\mathbf{R}_I) + \sum_i \frac{\mathbf{p}_i^2}{2m} + \sum_{i,I} u(\mathbf{r}_i, \mathbf{R}_I) + \sum_{i \neq j} \frac{e^2}{|\mathbf{r}_i - \mathbf{r}_j|}, \quad (1.12)$$

where $\mathbf{P}_I$ and M_I are the momentum and mass of I-th ions. $\mathbf{p}_i$ and m are the momentum and mass of the electrons. $V(\mathbf{R}_I) = \frac{e^2}{2} \sum_I \sum_{J \neq I} \frac{Z_I Z_J}{|\mathbf{R}_I - \mathbf{R}_J|}$ and $\frac{e^2}{|\mathbf{r}_i - \mathbf{r}_j|}$ are inter-nuclear and inter-electronic interactions respectively. $u(\mathbf{r}_i, \mathbf{R}_I) = e^2 \sum_{I=1} \sum_{i=1} \frac{Z_I}{|\mathbf{R}_I - \mathbf{r}_i|}$ is the electron-ion interaction potential. Here Z_I is the atomic number of the I-th ion. In the adiabatic approximation, we calculate the total energy $E_{e\mathbf{R}_I}$ of the electrons with a frozen-in configuration of the ions $\{\mathbf{R}_I\}$. The corresponding Hamiltonian for the electrons can be written as,

$$H_{e\mathbf{R}_I} = \sum_i \frac{\mathbf{p}_i^2}{2m} + \sum_{i,I} u(\mathbf{r}_i, \mathbf{R}_I) + \sum_{i \neq j} \frac{e^2}{|\mathbf{r}_i - \mathbf{r}_j|} \quad (1.13)$$

Now let us denote the wave function for the electronic part, at some ionic configuration $\mathbf{R}_I$, to be $\Phi_{\mathbf{R}_I}(\mathbf{r}_i)$ which satisfies the following equation,

$$H_{e\mathbf{R}_I} \Phi_{\mathbf{R}_I}(\mathbf{r}_i) = E_{e\mathbf{R}_I} \Phi_{\mathbf{R}_I}(\mathbf{r}_i) \quad (1.14)$$

Now we can write the total wave function which consists of both electronic part and ionic part for Eq. (1.12) as,

$$\Xi(\mathbf{R}_I, \mathbf{r}_i) = \Psi(\mathbf{R}_I)\Phi_{\mathbf{R}_I}(\mathbf{r}_i), \tag{1.15}$$

where $\Psi(\mathbf{R}_I)$ is the nuclear wave function. Putting Eq. (1.15) and Eq. (1.14) in Eq. (1.12) and rearranging the terms we find,

$$\begin{aligned}\mathcal{H}\Xi(\mathbf{R}_I, \mathbf{r}_i) = -\sum_I \frac{\hbar^2}{2M_I}\frac{\partial^2}{\partial \mathbf{R}_I^2}\Psi(\mathbf{R}_I)\Phi_{\mathbf{R}_I}(\mathbf{r}_i) + V(\mathbf{R}_I)\Psi(\mathbf{R}_I)\Phi_{\mathbf{R}_I}(\mathbf{r}_i) \\ + E_{e\mathbf{R}_I}\Psi(\mathbf{R}_I)\Phi_{\mathbf{R}_I}(\mathbf{r}_i),\end{aligned} \tag{1.16}$$

which upon simplification and regrouping, turns out to be [37] ,

$$\begin{aligned}\mathcal{H}\Xi(\mathbf{R}_I, \mathbf{r}_i) = \Phi_{\mathbf{R}_I}(\mathbf{r}_i)\Bigg[-\sum_I \frac{\hbar^2}{2M_I}\frac{\partial^2}{\partial \mathbf{R}_I^2} + V(\mathbf{R}_I) + E_{e\mathbf{R}_I}\Bigg]\Psi(\mathbf{R}_I) \\ -\sum_I \frac{\hbar^2}{2M_I}\Bigg[2\frac{\Psi(\mathbf{R}_I)}{\partial \mathbf{R}_I}\frac{\Phi_{\mathbf{R}_I}(\mathbf{r}_i)}{\partial \mathbf{R}_I} + \Psi(\mathbf{R}_I)\frac{\partial^2\Phi_{\mathbf{R}_I}(\mathbf{r}_i)}{\partial \mathbf{R}_I^2}\Bigg]\end{aligned} \tag{1.17}$$

We can verify that, Eq. (1.15) is the total wave function for the system within the adiabatic principle provided that the second part of Eq. (1.17) vanishes and $\Psi(\mathbf{R}_I)$ satisfies,

$$\Big[-\sum_I \frac{\hbar^2}{2M_I}\frac{\partial^2}{\partial \mathbf{R}_I^2} + V(\mathbf{R}_I) + E_{e\mathbf{R}_I}\Big]\Psi(\mathbf{R}_I) = E\Psi(\mathbf{R}_I), \tag{1.18}$$

where E is the total energy corresponding to the Hamiltonian $\mathcal{H}$. The adiabatic approximation thus gives a reliable estimate of total energy of a system and it dictates that electrons simultaneously follow the ionic motion always remaining in single state, namely the ground state. Now from the last term Eq. (1.17), we can define the electron-phonon coupling Hamiltonian as,

$$-\sum_I \frac{\hbar^2}{2M_I}\left[2\frac{\partial\Psi(\mathbf{R}_I)}{\partial\mathbf{R}_I}\frac{\partial\Phi_{\mathbf{R}_I}(\mathbf{r}_i)}{\partial\mathbf{R}_I}\right] = \mathcal{H}_{el-ph}\Psi(\mathbf{R}_I)\Phi_{\mathbf{R}_I}(\mathbf{r}_i), \tag{1.19}$$

which was dropped from the adiabatic Hamiltonian Eq. (1.17) because the expectation value of this term in any state such as Eq. (1.15) gives zero value. This term operates on both the electronic wave function as well on the phonon state and therefore corresponds to coupling between them. If electron-phonon coupling is large, then both the electronic configuration as well as the ionic configuration are altered. The adiabatic approximation which allow the electronic wave function to remain unaltered must be modified to allow for these transitions because the electronic wave function which are continuously deformed by the ionic motions may shift their orbital as a consequence of electron scattering. Generally, modification of electronic states are not necessary when the period of lattice vibration is smaller than the electronic relaxation time τ. In this situation, a given electron should be known to persists in the same state for many oscillations of the ions and hence the change of electronic states are not viable.

The matrix elements for electron-phonon scattering can be calculated with the help of time-dependent perturbation theory. To simplify the problem,

we assume single particle wave function $\psi_{\mathbf{ki}}(\mathbf{r})$ which can be scattered from state $\mathbf{k}$ to $\mathbf{k'}$ and assume a phonon state $\boldsymbol{\eta}_{\mathbf{q},p}$ of lattice wave vector $\mathbf{q}$ and polarization p. The matrix element can now be written as [37],

$$\mathcal{M}(\mathbf{k},\mathbf{k'}) = \langle \boldsymbol{\eta}_{\mathbf{q},p}| \int \psi_{\mathbf{k}^* j} \mathcal{H}_{el-ph} \psi_{\mathbf{k'}i} d\mathbf{r} \, |\boldsymbol{\eta}_{\mathbf{q},p} - 1\rangle \tag{1.20}$$

The action of the Hamiltonian operator $\mathcal{H}_{el-ph}$ is made simple by Blöch function. When the ions moves with the lattice vibration in a crystal, the potential energy as seen by the electron is changed by $\boldsymbol{\delta}\mathbf{u}$. This change in potential act as a perturbation and has the effect to scatter the electrons into new states due to electron-phonon interaction. So we can write,

$$\boldsymbol{\delta}\mathbf{u} = \sum \boldsymbol{\eta}_{\mathbf{l},b} . \frac{\partial u(\mathbf{r})}{\partial \boldsymbol{\eta}_{\mathbf{l},b}}, \tag{1.21}$$

where $\boldsymbol{\eta}_{\mathbf{l},b}$ is the ionic displacement operator which acts on phonon states and is a function of ions position at $(\mathbf{l},\mathbf{b})$. $\mathbf{l}$ is the reciprocal lattice vector and $\mathbf{b}$ is the ionic coordinate. Using Eq. (1.21) in Eq. (1.20), we can write the matrix element in Dirac's Bra-ket notation as follows,

$$\mathcal{M}(\mathbf{k},\mathbf{k'}) = \langle \mathbf{k}+\mathbf{q}, i| \, \Delta u_{\mathbf{q},p} \, |\mathbf{k}, j\rangle \, , \tag{1.22}$$

where the derivative of the potential is with respect to ionic displacement of the lattice. We will see consequences of this equation in later chapter of this thesis. As said earlier, the crystal momentum will be conserved in any such scattering phenomena and the relation is expressed by the condition,

$$\mathbf{q} = \mathbf{k'} - \mathbf{k} - \mathbf{g}$$

Where **g** is an arbitrary vector of the reciprocal lattice. When **g** is not zero, we call it *Umklapp scattering*.

Bibliography

[1] T. Aoyama, M. Hayakawa, T. Kinoshita and M. Nio, Phys. Rev. Lett. **109**, 111807 (2012).

[2] M. C. Payne, M. P. Teter, D. C. Ailan, T. A. Arias and J. D. Joannopouios, Rev. Mod. Phys. **64**, 1045 (1992).

[3] J. Ihm, Rep. Prog. Phys. **51**, 105 (1988).

[4] J. Kohanoff, Electronic Structure Calculations for Solids and Molecules, Cambridge University Press, Cambridge (2006), ISBN:13-978-0-521-81591-8.

[5] R. M. Martin, Electronic Structure, Basic Theory and Practical Methods, Cambridge University Press, Cambridge (2004), ISBN: 978-0-521-78285-6.

[6] F. Bloch, Z. Phys. **52**, 555 (1928).

[7] A. H. Wilson, Proc. Roy. Soc. A **133**, 458 (1931).

[8] A. H. Wilson, Proc. Roy. Soc. A **134**, 277 (1931).

[9] W. Kohn, Phys. Rev. A **171**, 133 (1964).

[10] R. Resta, Ferroelectrics **51**, 136 (1992).

[11] R. D. King-Smith and D. Vanderbilt, Phys. Rev. B **47**, 1651 (1993).

[12] R. Resta, Rev. Mod. Phys. **66**, 899 (1994).

[13] R. Resta, Eur. Phys. J. B **79**, 121 (2011).

[14] C. L. Kane and E. J. Mele, Phys. Rev. Lett. **95**, 226801 (2005).

[15] F. D. M. Haldane, Phys. Rev. Lett. **61**, 2015 (1988).

[16] B. A. Bernevig, T. L. Hughes and S. C. Zhang, Science **314**, 1757 (2006).

[17] M. Knig, S. Wiedmann, C. Brne, A. Roth, H. Buhmann, L. W. Molenkamp, X. L. Qi and S. C. Zhang, Science **318**, 766 (2007).

[18] J. Linder, Y. Tanaka, T. Yokoyama, A. Sudb, and N. Nagaosa, Phys. Rev. Lett. **104**, 067001 (2010).

[19] A. Cook and M. Franz, Phys. Rev. B **84**, 201105(R) (2011).

[20] C. Nayak, S. H. Simon, A. Stern, M. Freedman and S. D. Sarma, Rev. Mod. Phys. **80**, 1083 (2008).

[21] M. Kim, C. H. Kim, H.-S. Kim, and J. Ihm, Proc. Natl. Acad. Sci. U.S.A. **109**, 671 (2012).

[22] S. Y. Xu, Y. Xia, L. A. Wray, S. Jia, F. Meier, J. H. Dil, J. Osterwalder, B. Slomski, A. Bansil, H. Lin, R. J. Cava and M. Z Hasan, Science **332**, 560 (2011).

[23] M. Bahramy, B. J. Yang, R. Arita and N. Nagaosa, Nat. Commun. **3**, 679 (2012).

[24] I. Garate, Phys. Rev. Lett. **110**, 046402 (2013)

[25] X. L. Qi, T. Hughes and S. C. Zhang, Phys. Rev. B **78**, 195424 (2008).

[26] M. Z. Hasan and C. L. Kane, Rev. Mod. Phys. **82**, 3045 (2010).

[27] L. Fu, C. L. Kane and E. J. Mele, Phys. Rev. Lett. **98**, 106803 (2007).

[28] J. E. Moore and L. Balents, Phys. Rev. B **75**, 121306(R) (2007).

[29] H. Suzuura and T. Ando, Phys. Rev. Lett. **89**, 266603 (2002).

[30] K. Nomura, M. Koshino and S. Ryu, Phys. Rev. Lett. **99**, 146806 (2007).

[31] E. Pyykko, Chem. Rev. **88**, 563 (1988).

[32] N. E. Christensen, Int. J. Quantum Chem. **25**, 233 (1984).

[33] S. Kupratakuln, J. Phys. C: Solid State Phys. **3**, S10 (1970).

[34] V. S. Mathur and S. Singh, Concepts in Quantum Mechanics, CRC Press, Boca Raton (2009), ISBN: 1420078720.

[35] B. H. Bransden and C. J. Joachim, Physics of Atoms and Molecules, Pearson Education Limited, England (1983), ISBN: 0582-35692-X.

[36] M. S. Dresselhaus, G. Dresselhaus and A. Jorio, Group Theory, Applicatioin to the Physics of Condensed Matter, Springer, Heidelberg (2008), ISBN-978-3-540-32897-1.

[37] Z. M. Ziman, Electrons and Phonons, Oxford University Press, Oxford (1960), ISBN: 978-0-19-850779-6.

[38] H. Zhang, C. X. Liu, X. L. Qi, X. Dai, Zhong Fang and S. C. Zhang, Nature Physics **5**, 438 (2009).

Chapter 2

Theoretical methodologies

In this chapter I will briefly discuss the theoretical background involved in the density functional theory. First I will give a formal description for calculating the total energy as prescribed within the density functional theory with and without the inclusion of relativistic effect. Then I will discuss about the pseudopotential approach with an emphasis on the norm-conserving pseudopotentials which form the basis of all the calculations performed in preparing this thesis. Finally, I will spent few minutes on frozen phonon approach and density functional perturbation theory (DFPT) which have been used to calculate the vibrational frequencies.

2.1 Simplifying the structure of a matter

The full Hamiltonian of a material consisting of electrons and ions as given in Eq.(1.12) can be rewritten in a more elaborative way as,

$$\begin{aligned}\mathcal{H} = -\sum_I \frac{\hbar^2}{2M_I}\nabla_I^2 - \sum_i \frac{\hbar^2}{2m}\nabla_i^2 + \frac{e^2}{2}\sum_I\sum_{J\neq I}\frac{Z_I Z_J}{|\mathbf{R}_I - \mathbf{R}_J|} \\ + \frac{e^2}{2}\sum_i\sum_{j\neq i}\frac{1}{|\mathbf{r}_i - \mathbf{r}_j|} - e^2\sum_{I=1}\sum_{i=1}\frac{Z_I}{|\mathbf{R}_I - \mathbf{r}_i|}\end{aligned} \tag{2.1}$$

Given this total Hamiltonian of any system, we can write the time-independent Schrödinger equation as,

$$\mathcal{H}\Xi(\mathbf{R}_I, \mathbf{r}_i) = E\Xi(\mathbf{R}_I, \mathbf{r}_i), \tag{2.2}$$

where $\Xi(\mathbf{R}_I, \mathbf{r}_i)$ is the total wave function as discussed earlier. All the properties (ground state) can be derived if we can solve the Eq. (2.2). But as a material has a very large number of ions and electrons and their degree of freedoms are coupled to each other, we will have a very complicated coupled differential equation which will be impossible to solve, no matter how powerful a computer we have, unless we resort to some reasonably good approximations.

2.1.1 Adiabatic approximation

As already discussed earlier, the adiabatic approximation (*Born-Oppenheimer* approximation [1]) is the most important assumption made to simplify the calculation of electronic structure of matters. This assumption has been made observing the fact that time scale associated with the motion of the

nuclei (ions) are much slower than that associated with electrons. Therefore electrons instantaneously follow the motion of the ions while remaining in the same stationary (adiabatic) state (ground or excited) without causing non-radiative transition by the nuclear dynamics. If this condition is followed then the dynamics is said to be adiabatic. The first quantity in the second expression of Eq. (1.17) which is responsible for the non-adiabatic effects in the system, is inversely proportional to energy difference between the adiabatic electronic eigenstates (*i.e.* band gap) and thus can be ignored if the energy gap is large. Thus in those large band gap systems adiabatic *Born-Oppenheimer* approximation holds good. But in systems with smaller band gaps, the *Born-Oppenheimer* approximation may break down. One example of such systems is graphene [2]. We will see consequences of broken adiabaticity in the third chapter in the case of Sb_2Se_3.

The electronic Hamiltonian of a system can be written in a short notation as,

$$H_e = T_e + U_{ee} + u(\mathbf{r}_i, \mathbf{R}_I) = \mathcal{H} - T_n - V(\mathbf{R}_I), \tag{2.3}$$

where T_e, T_n are the kinetic energies of electrons and nuclei respectively. $U_{ee}(= \sum_{i \neq j} \frac{e^2}{|\mathbf{r}_i - \mathbf{r}_j|})$ and $V(\mathbf{R}_I)$ are electron-electron and nuclear-nuclear interaction potential respectively. $u(\mathbf{r}_i, \mathbf{R}_I)$ is the interaction potential between the electrons and nuclei. $\mathcal{H}$ is the total Hamiltonian of the system.

2.1.2 Classical nuclei approximation

The nuclear masses are quite heavy as compared to electrons, so the wave functions for nuclei are much more localized. Therefore one can harmlessly assume that quantum phase coherence of the nuclear wave functions is very less or doest not exist at all and we can safely treat nuclei as classical particles. This is known as *classical nuclei approximation* which is the second most important assumption made in simplifying the electronic structure of a matter. Within this approximation, we can write the total nuclear wave function as the product of all individual nuclear wave function and therefore we can neglect the exchange and correlation interactions among them.
The dynamics of the mean values of position and momentum operators can be obtained through Ehrenfest's theorem as follows,

$$i\hbar\frac{d\langle\mathbf{R}\rangle}{dt} = \langle[\mathcal{H},\mathbf{R}]\rangle = i\hbar\frac{\langle\mathbf{P}\rangle}{M} \Rightarrow M\frac{d\langle\mathbf{R}\rangle}{dt} = \langle\mathbf{P}\rangle \tag{2.4}$$

$$i\hbar\frac{d\langle\mathbf{P}\rangle}{dt} = \langle[\mathcal{H},\mathbf{P}]\rangle = -i\hbar\langle\nabla E_e(\mathbf{R})\rangle, \tag{2.5}$$

where $\mathbf{R}$ and $\mathbf{P}$ are position and momentum operators respectively. E_e is the total energy corresponding to the electronic Hamiltonian Eq. (2.3). Combining those above two equations, we can arrive at the very familiar Newton's equation of motion,

$$M\frac{d^2\langle\mathbf{R}\rangle}{dt^2} = -\langle\nabla E_e(\mathbf{R})\rangle \tag{2.6}$$

From the *Hellmann-Feynman* theorem [3], we know that the variation of the electronic energy with respect to any external parameter λ coupled to the electrons, can be computed as,

$$\frac{\partial E_e(\lambda)}{\partial\lambda} = \left\langle \phi_{\mathbf{R}_I}(\mathbf{r}) \middle| \frac{\partial H_e(\lambda)}{\partial\lambda} \middle| \phi_{\mathbf{R}_I}(\mathbf{r}) \right\rangle, \tag{2.7}$$

where $\phi_{\mathbf{R}_I}(\mathbf{r})$ is the electronic wave function for the nuclear configuration $\{\mathbf{R}_I\}$. If $E_{PES}(\mathbf{R}_I) = E_e(\mathbf{R}_I) + V(\mathbf{R}_I)$ can be defined as the potential energy surface (PES) of any system for some ionic configurations $\{\mathbf{R}_I\}$, then together with the help of Eq. (2.6) and Eq. (2.7), we can write for $\lambda = \mathbf{R}_I$,

$$M_I\frac{d^2\langle\mathbf{R}_I\rangle}{dt^2} = -\left\langle \phi_{\mathbf{R}_I}(\mathbf{r}) \middle| \frac{\partial H_e(\lambda)}{\partial\lambda} \middle| \phi_{\mathbf{R}_I}(\mathbf{r}) \right\rangle - \frac{\partial V(\mathbf{R}_I)}{\partial\mathbf{R}_I}. \tag{2.8}$$

The solution of the stationary problem *i.e.* $\nabla E_{PES}(\mathbf{R}_I) = 0$ to find the minimum force on each ion through Eq. (2.7) is known as *geometry optimization* of a system. But first of all, we have to determine the total electronic energy $E_e(\mathbf{R}_I)$ of the system. Solving the time independent Schrödinger equation to get $E_e(\mathbf{R}_I)$ is known by the name of *electronic structure calculation*.

2.1.3 Independent electron approximation

There are two basic independent-particle approaches that may be categorized into "non-interacting" or *Hartree* method and *Hartree-Fock* method. In *Hartree* method, only the classical electrostatic Coulomb interaction energy is taken into account while neglecting the exchange and correlation effect. But in *Hartree-Fock* method, in addition to the electrostatic interaction energy, the exchange effect due to Pauli principle and correlation effect are taken into account. In modern DFT, the electronic Hamiltonian is taken to be non-interacting like in *Hartree* approach and electrons are assumed to move in an effective external potential chosen so as to incorporate the exchange-correlation effect approximately which is always present in a true many-body wave function. In the next section I will discuss about the exchange and correlation effect.

2.1.4 Exchange and correlation effect

exchange-interaction is a quantum mechanical interaction between identical particles. For the electrons which obey *Fermi-Dirac* statistics, exchange interaction arises due to Pauli principle. For example, let us assume that an spin-up electron stays at the origin of a system. Pauli principle forbids the presence of another spin-up electron at that place but tells nothing about spin-down electron which is perfectly allowable. This phenomena is known as *exchange interaction* and it can be taken care of by writing the many body wave function in Slater determinant.

Within the *Hartree-Fock* theory, the wave function for a many body system

can be written in terms of single particle waves in Slater determinant while keeping in mind the antisymmetry nature of the electronic orbitals. A single Slater determinant, however, could not capture the true Coulomb interaction among the electrons. Thus, this approach assumes some kind of separability of the Schrödinger equation, implying that the probability of finding an electron at some points in space is independent of the location of other electrons. So, it neglects the electron-electron repulsion which is always present in a realistic system. The probability of finding an electron at position **r** depends on the location of other electrons. This phenomenon is known as the *correlation* effect.

2.2 Density functional theory

There exist many methods in the literature for calculating the electronic structure of a system. Among the existing most popular ones, physicists prefer density functional theory over other approaches like *Hartree-Fock* method which is mostly favored by the chemists, because of its many computational advantages. Here I will concentrate only on density functional theory which I have used in all the calculations. The main idea of density functional theory is that it casts the interacting many-body problem into single particle problem via the particle density with the many-body effects included in the exchange-correlation functional. It is based on two powerful theorems given by Hohenberg & Kohn [4] and Kohn & Sham [5] which state that the total energy of a system is a unique functional of its ground state electron density. The development of density functional theory began with the idea of L.

H. Thomas and E. Fermi who, at about the same time of Hartree, thought the full electronic density as a fundamental variable in many body problems rather than the many-body wave function itself. This approximation is known as *Thomas-Fermi* approximation. Although it was too crude to be used in actual problems because of its many limitations, it sets up the basis of modern *density functional theory* (DFT).

2.2.1 Thomas-Fermi theory

Thomas and Fermi constructed the total electronic energy of an inhomogeneous system as a functional of electron density ρ as given below,

$$E_\alpha[\rho] = \int \rho(\mathbf{r})\epsilon_\alpha[\rho(\mathbf{r})]d\mathbf{r}, \tag{2.9}$$

where $\epsilon_\alpha[\rho(\mathbf{r})]$ is the energy density which consists of the contributions (α) from kinetic, exchange and correlation energy of a homogeneous electron gas for which good approximations already exist. This energy density is calculated locally at every point and integrated over whole space. In some sense, this is a kind of *local density approximation* (LDA). The above expression in the square bracket of Eq. (2.9) is called a functional which depends on some function (here it is the electron density $\rho(\mathbf{r})$). For a homogeneous electron gas, we know that the electron density (ρ) and kinetic energy density ($t[\rho]$) are given by,

$$\begin{cases} \rho = \frac{1}{3\pi^2}\left(\frac{2m}{\hbar^2}\right)^{3/2}\epsilon_F^{3/2} \\ t[\rho] = \frac{3}{5}\frac{\hbar^2}{2m}(3\pi^2)^{2/3}\rho^{2/3}, \end{cases} \tag{2.10}$$

where ϵ_F is the Fermi energy. Therefore the total kinetic energy (T_{TF}) according to *local density approximation* of Thomas & Fermi can be written as,

$$T_{TF} = C_k \int \rho(\mathbf{r})^{5/3} d\mathbf{r}, \tag{2.11}$$

with $C_k = 3(3\pi^2)^{2/3}/10$.

The exchange and correlation were introduced in the same local spirit by Dirac [6] and Wigner [7] respectively and are given by,

$$E_X[\rho] = -C_X \int \rho(\mathbf{r})^{4/3} d\mathbf{r} \tag{2.12}$$

$$E_C[\rho] = -a \int \frac{\rho(\mathbf{r})^{4/3} d\mathbf{r}}{b + \rho(\mathbf{r})^{1/3}}, \tag{2.13}$$

where $C_X = 3(3/\pi)^{1/3}/4$. a, b are numerical constants. When exchange interaction is included, the theory is called *Thomas-Fermi-Dirac* approximation. Finally the total electronic energy according to the *Thomas-Fermi-Dirac* theory as a functional of electron density can be written as,

$$E_{TFD}[\rho] = C_k \int \rho(\mathbf{r})^{5/3} d\mathbf{r} + \int \rho(\mathbf{r}) \nu_{ext}(\mathbf{r}) d\mathbf{r} + \frac{1}{2} \iint \frac{\rho(\mathbf{r})\rho(\mathbf{r'})}{|\mathbf{r} - \mathbf{r'}|} - C_X \int \rho(\mathbf{r})^{4/3} d\mathbf{r} + E_C[\rho], \tag{2.14}$$

where $\int \rho(\mathbf{r}) \nu_{ext}(\mathbf{r}) d\mathbf{r} = V_{ext}$ is the external field–a generalization of the electron-nuclear interaction defined in the previous chapter.

2.2.2 Hohenberg-Kohn theorem

The modern density functional theory stands upon two powerful theorems given by Hohenberg & Kohn [4] who formulated DFT as an exact many-body theory of a many-body system. The formulation of DFT applies to any interacting system whose particles are assumed to move in an external potential $V_{ext}(\mathbf{r})$. The Hamiltonian of such systems can be written as,

$$H_e = T_e + V_{ext}(\mathbf{r}) + U_{ee}(\mathbf{r}) \tag{2.15}$$

First Hohenberg-Kohn theorem - For any system of interacting particles in an external potential $V_{ext}(\mathbf{r})$, the potential $V_{ext}(\mathbf{r})$ is uniquely determined by the ground state electronic density $\rho_0(\mathbf{r})$ of the system within the ambiguity of an additive constant.

Second Hohenberg-Kohn theorem - A universal functional of energy $E[\rho]$ can be defined corresponding to any external potential $V_{ext}(\mathbf{r})$. The ground state energy of a system is the global minimum of this functional.

The electronic density $\rho(\mathbf{r})$ which minimizes the functional is called ground state density $\rho_0(\mathbf{r})$ of the system.

2.2.3 Kohn-Sham approach

Having established the basic formulas, the problem arises in casting the many-body theory in a tractable scheme based on the *Hohenberg-Kohn* theorems where the total energy is an unknown functional of density. The problem, however, was solved by Kohn & Sham [5] who assumed the system consisting of non-interacting electrons in an external potential. This is the central theme of Kohn-Sham approach to density functional theory. In their approach, the unknown Hohenberg-Kohn functional is nothing but the kinetic energy of the electrons. The idea of Kohn-Sham was that if one can find any non-interacting electronic system that produces the same electronic density as that of the interacting system, then the kinetic energy of the electrons can be calculated through one electron orbitals. Though the kinetic energy calculated in this way will not be exactly same as that of the kinetic energy obtained from a many-body wave function. The missing fraction is due to the *correlation* among the electrons which can be approximately included in the exchange-correlation functional. The ground state density matrix, in terms one electron orbital, can be written as,

$$\rho(\mathbf{r}, \mathbf{r'}) = \sum_i f_i \phi_i(\mathbf{r}) \phi_i^*(\mathbf{r'}), \tag{2.16}$$

where f_i are the occupations of the one electron orbitals $\phi_i(\mathbf{r})$. So the kinetic energy of the non-interacting system can be cast into form,

$$T_e = -\frac{\hbar^2}{2m} \sum_i f_i \langle \phi_i | \nabla^2 | \phi_i \rangle \tag{2.17}$$

Let us assume that the reference potential for the non-interacting system be $\nu_R(\mathbf{r})$ with one electron orbital $\phi_i(\mathbf{r})$. The electron density of this system (non-spin polarized) becomes $\rho(\mathbf{r}) = 2\sum_i |\phi_i(\mathbf{r})|^2$, while the kinetic energy is

$$T_e = -\frac{\hbar^2}{m} \sum_i \langle \phi_i | \nabla^2 | \phi_i \rangle \tag{2.18}$$

The Kohn-Sham one electron Hamiltonian can then be written as,

$$H_e = -\frac{\hbar^2}{2m}\nabla^2 + \nu_R(\mathbf{r}), \tag{2.19}$$

where $\nu_R(\mathbf{r})$ is the potential for the reference system and will be defined shortly. With the above equations for the non-interacting reference system, the *Kohn-Sham* functional can be written as,

$$E_{KS}[\rho] = T_R[\rho] + \int \rho(\mathbf{r})\nu_{ext}(\mathbf{r})d\mathbf{r} + \frac{1}{2}\iint \frac{\rho(\mathbf{r})\rho(\mathbf{r'})}{|\mathbf{r}-\mathbf{r'}|} d\mathbf{r}d\mathbf{r'} + E_{XC}[\rho], \tag{2.20}$$

where $T_R[\rho]$ is the kinetic energy of the electrons in the non-interacting reference system. The minimization of the Eq. (2.20) with respect to density ρ, subject to the constraint that electron density integrates out to total number of electron in the system, will lead to ground state energy of the system. After few lines of mathematical derivations, the reference potential can be written as,

$$\begin{aligned} \nu_R(\mathbf{r}) &= \nu_{ext}(\mathbf{r}) + \iint \frac{\rho(\mathbf{r'})}{|\mathbf{r}-\mathbf{r'}|} d\mathbf{r'} + \mu_{XC}[\rho(\mathbf{r})] \\ \text{with,} \qquad \mu_{XC}[\rho(\mathbf{r})] &= \frac{dE_{XC}[\rho]}{d\rho(\mathbf{r})} \end{aligned} \tag{2.21}$$

This equation has to be solved self-consistently making sure that the density used to construct the reference potential matches (*i.e.* self-consistent) with that obtained from solving the Kohn-Sham Hamiltonian Eq. (2.19) via $\rho(\mathbf{r}) = 2\sum_i |\phi_i(\mathbf{r})|^2$.

2.2.4 Approximation to exchange & correlation

One of the main difficulties in density functional theory is to formulate a correct exchange-correlation functional. Among all the existing functionals , local density approximation (LDA) and generalized gradient approximation (GGA) are the most popular and widely used.

In LDA, the effect of exchange and correlation are considered to be local in nature as it was assumed by Kohn & Sham in their seminal paper [5]. In this approach, the inhomogeneous system is thought to be locally homogeneous and exchange-correlation energy can be obtained simply by integrating the

exchange-correlation energy density at each point over all space. This density is known very accurately for homogeneous electron gas [6] and considered to be same at each point in the system. The exchange-correlation energy in LDA is thus given by,

$$E_{xc}^{LDA}[\rho] = \int d^3\mathbf{r}\rho(\mathbf{r})\epsilon_{xc}^{homo}[\rho(\mathbf{r})] \tag{2.22}$$

The LDA approximation proves to be very successful for many systems especially for those whose electron density is quite uniform such as bulk metals, ionic crystals etc. But it fails to produce some properties (e.g. band gap) in semiconductors, strongly correlated systems due to fact that the excitation spectrum of homogeneous electron gas is gap-less and exchange-correlation energy is regular [8]. LDA also fails to capture weak inter-molecular bonds, hydrogen bonds etc.

The improvement of LDA leads to the development of GGA where several aspects which were not present in LDA like inhomogeneity of electrons, non-local exchange correlation effect, complete cancellation of self-energies of electrons are taken into account. In general the exchange-correlation energy in GGA can be written as [9],

$$E_{xc}^{GGA}[\rho] = \int d^3\mathbf{r}\rho(\mathbf{r})\epsilon_{xc}[\rho(\mathbf{r}), |\nabla\rho|, |\nabla^2\rho|, ...] \tag{2.23}$$

The GGA method turns out to be better than LDA in the sense that it improves binding energies, bond lengths. Semiconductors are better described in GGA than LDA. GGA also improves the band gap of semiconductors over LDA. For all these reasons, we throughly use GGA as exchange-correlation functional in all the *ab-initio* calculations described in this thesis.

2.2.5 Pseudopotentials

The wave function for free electrons can be expanded in terms of plane waves and without the presence of any atomic potential these plane waves are the exact solutions to the Schrödinger equation. But the situation in a real crystal is far different than the case of free electrons. Due to presence of inter-nuclear potential, the wave function for an atom shows oscillatory behavior in the core region. As the interaction between the core ionic state and the valence electrons increases, the wave function in the core region become more oscillatory with more number of nodes. Then, to express a true wave function with plane waves, we need in principle an infinite number of plane wave components. This makes the diagonalization of the Hamiltonian matrix almost impossible. To recover from this problem a number of recipes were proposed like *augmented plane wave* (APW) [10] method where the plane wave expansion was augmented with the solutions of the atomic problem in a spherical region around the atoms and the potential outside this sphere is assumed to be zero. Another approach, called *orthogonalized plane wave* (OPW) method was proposed by Herring [11] who expanded the valence states as a linear combination of plane waves and the core states and choose

the coefficients so as to make the resultant wave function orthogonal to that of the core states.

Pseudopotential approximation is one step further modification of the OPW method. Identifying the fact that in a material it is the valence electrons which take part in bonding and other chemical activity and core electrons sit idle, one can replace the interaction between the core region (which consists of nuclei and core electrons) and the valence electrons with a smooth effective potential which can accurately produce the bonding properties of the true potential. In this smooth potential region one can construct a nodeless wave function (pseudo wave function) which needs very small number of plane waves to be expanded and thus rendering the diagonalization of the Hamiltonian very easy.

The modern pseudopotential theory is due to Philips & Kleinman [12] who showed that one can construct a valence wave function $\tilde{\phi}_v$ which is not orthogonal to the core wave states (ϕ_c) by combining the core and true valence wave function (ϕ_v) in the following way,

$$|\tilde{\phi}_v\rangle = |\phi_v\rangle + \sum_c \alpha_{cv} |\phi_c\rangle \,, \tag{2.24}$$

where $\alpha_{cv} = \langle\phi_c|\tilde{\phi}_v\rangle \neq 0$. This pseudo wave function satisfies the following pseudo Hamiltonian which has same eigenvalue as the original Hamiltonian.

$$\left[\mathcal{H} + \sum_c (\epsilon_v - \epsilon_c) \left|\phi_c\right\rangle \left\langle\phi_v\right|\right] \left|\tilde{\phi}_v\right\rangle = \epsilon_v \left|\tilde{\phi}_v\right\rangle , \tag{2.25}$$

where $\mathcal{H} = T + V$, $V = (Z_C/\mathbf{r})$ is the bare Coulomb potential. Now we can define the pseudopotential as,

$$V_{PS} = \frac{Z_c}{\mathbf{r}} + \sum_c (\epsilon_v - \epsilon_c) \left|\phi_c\right\rangle \left\langle\phi_c\right| \tag{2.26}$$

2.2.6 Norm-conserving pseudopotential

Norm-conserving pseudopotential is very important among all the *ab-initio* pseudopotentials. It makes calculation more accurate as well the makes the pseudopotential more transferable. The definition of a norm-conserving pseudopotential as give by Hamann, Schlüter & Chiang [13] are following,

i) The eigenvalues of the pseudo-wave function match with that of all-electron wave function for a chosen configuration of the atom.

ii) All-electron wave function and pseudo wave function are identical outside a chosen cut-off radius r_c

iii) The norm of the true wave function and all-electron wave function are the same inside the pseudized region ($r < r_c$).

iv) The logarithmic derivative of the all-electron wave function and the pseudo wave function agree for $r \geq r_c$.

The last condition has very important implications. The small change in

the eigenvalues due to external potential (i.e when environment of a particular atom changes from one system to another) produce only second-order changes in the logarithmic derivatives. This implies that the electronic eigenvalues are shifted from their atomic values in a different environment but the transferability property ensures that all-electron and pseudo wave function still coincide outside the cut-off radii.

One frequently encountered problem with norm-conserving pseudopotential is that its hard-ness. The norm-conserving constraint ensures that the pseudo charge has to match with all-electron charge thus requiring a large number of plane waves making the pseudopotential hard for any practical calculation. To get rid of this "hard-ness", another type of pseudopotential has been created which is called ultrasoft pseudopotential (USPP) [14].

2.3 Phonons

In solid state physics, very often we describe a material as a gas of collective excitations. For example, to explain the electrical conductivity of a material we describe it consisting of electron gas. The thermal conductivity of material is explained through collective excitations of lattice vibrations and so on. In fact, to explain any physical phenomena in a very small time scale, we need to consider collective behavior arising from all particles inside a matter instead of individual particle model. An example of such successful collective particles model is the Einstein model in which thermal conductivity of solid is assumed to be distributed among all the normal modes of vibrations in the whole crystal. Einstein model can accurately predict the specific heat in

solid. These normal modes in solid arise due to the vibration of the atoms in their lattice sites. As quanta of electromagnetic radiation is called photon, the quanta of lattice vibration is similarly called phonon. Another important aspect of phonon is that if we want to compute any thermodynamical quantity of a crystal from *first-principles* calculation at finite temperature, then we have to approximately calculate the vibrational entropy or energy from the phonon density of states. Thus the phonon frequencies of a crystal can reveal very interesting physics and insightful dynamical informations in a system. Now-a-days, with the availability of powerful computers and sophisticated algorithms, the phonon dispersions of materials are routinely studied.

Here we will discuss two such approaches to calculate the phonon frequencies of a system within the adiabatic density functional theory- frozen phonon approach and density functional perturbation theory.

2.3.1 Frozen-phonon approach

Frozen-phonon approach is a very easy and computationally inexpensive practical method to calculate the normal modes of lattice vibrations (or phonon frequencies). In this approach, we displace each atom in the unit cell of the crystal to some extent and calculate the force on them with the help of density functional theoretical calculation using the *Hellman-Feynman* theorem. We construct the force constant matrix collecting forces from all the atoms and convert it to dynamical matrix with the help of Fourier transformation which, then, can be solved at any $\mathbf{q}$ point in the Brillouin zone to

get the phonon frequencies.

Another very accurate method, based on the linear response theory exists to calculate the frequencies of lattice vibration, is the *density functional perturbation theory* which will be discussed in the next subsection.

2.3.2 Density functional perturbation theory

Lattice-dynamical properties of a system are not only related to the lattice vibrations but also it has some profound electronic connections. The modern theory of lattice vibrations are firmly based on the linear response theory formulated by Pick et el. [15]. The combination of state-of-the art density functional theory and linear response theory gives rise to what is known as the density functional perturbation theory [16,17]. Now we will discuss the basic mathematical formulations of this theory. Adiabatic *Born-Oppenheimer* approximation helps in decoupling the electronic degrees of freedom from that of the vibrational degrees. The equation which arises due to this theorem is written in Eq. (1.18) as,

$$\Big[-\sum_I \frac{\hbar^2}{2M_I}\frac{\partial^2}{\partial \mathbf{R}_I^2} + V(\mathbf{R}_I) + E_{e\mathbf{R}_I} \Big] \Psi(\mathbf{R}_I) = E\Psi(\mathbf{R}_I), \tag{2.27}$$

The lattice-dynamical properties of any system is given by the eigenvalue E and eigenfunction $\Psi(\mathbf{R}_I)$ of this equation. The energy $E_{e\mathbf{R}_I}$ is the ground state energy of the interacting electrons moving in the field of fixed nuclei and is often referred to as *Born-Oppenheimer energy surface*. The Hamiltonian corresponding to this energy surface acts on the electronic variables

which depend parametrically on the nuclear coordinates $\mathbf{R}_I$. The equilibrium geometry of the system or *geometry optimization* is given by the condition that force acting on each atom should be minimum and this is written mathematically as,

$$F_I = -\frac{\partial E_{e\mathbf{R}_I}}{\partial \mathbf{R}_I} \tag{2.28}$$

The vibrational frequencies of a system is obtained from the Hessian of the $E_{e\mathbf{R}_I}$ after being scaled properly by the nuclear masses. The Hessian matrix can be written as,

$$det\left|\frac{1}{\sqrt{M_I M_J}}\frac{\partial^2 E}{\partial \mathbf{R}_I \partial \mathbf{R}_J} - \omega^2\right| = 0 \tag{2.29}$$

The forces on the atoms or the first order derivative of energy can be obtained accurately by the *Hellman-Feynman* theorem with the help of Eq. (2.7) and Eq. (2.8). The *Born-Oppenheimer* Hamiltonian depends on the nuclear coordinates through the electron-nuclear interaction and it couples to the electrons through electronic charge density. In terms of electronic charge density Eq. (2.7) can be written as,

$$F_I = -\int \rho_{\mathbf{R}_I}(\mathbf{r})\frac{\partial u(\mathbf{r}_i, \mathbf{R}_I)}{\partial \mathbf{R}_I} d\mathbf{r} - \frac{\partial V(\mathbf{R}_I)}{\partial \mathbf{R}_I}, \tag{2.30}$$

where $\rho_{\mathbf{R}_I}(\mathbf{r})$ is the ground state electronic density corresponding to nuclear configuration $\{\mathbf{R}_I\}$. The double derivative of $E_{e\mathbf{R}_I}$ yields,

$$\begin{aligned}\frac{\partial^2 E_{\mathbf{R}_I}}{\partial \mathbf{R}_I \partial \mathbf{R}_J} &= -\frac{\partial F_I}{\partial \mathbf{R}_J} \\ &= \int \frac{\partial \rho_{\mathbf{R}_I}(\mathbf{r})}{\partial \mathbf{R}_J} \frac{\partial u(\mathbf{r}_i, \mathbf{R}_I)}{\partial \mathbf{R}_I} d\mathbf{r} + \int \rho_{\mathbf{R}_I}(\mathbf{r}) \frac{\partial^2 u(\mathbf{r}_i, \mathbf{R}_I)}{\partial \mathbf{R}_I \partial \mathbf{R}_J} d\mathbf{r} + \frac{\partial^2 V(\mathbf{R}_I)}{\partial \mathbf{R}_I \partial \mathbf{R}_J},\end{aligned} \tag{2.31}$$

where $u(\mathbf{r}_i, \mathbf{R}_I)$ is the electron-nuclear interaction and $V(\mathbf{R}_I)$ is nuclear-nuclear interaction. From the above matrix we see that, the Hessian matrix or the force constant matrix requires ground state electronic charge density $\rho_{\mathbf{R}_I}(\mathbf{r})$ as well the *linear response* of it under under the perturbation of nuclear geometry. Hence the name *linear response theory*.

Bibliography

[1] M. Born and J. R. Oppenheimer, Ann. Physik **84**, 457 (1927).

[2] S. Pisana, M. Lazzeri, C. Casiraghi, K. S. Novoselov, A. K. Geim, A. C. Ferrari and F. Mauri, Nature Materials **6**, 198 (2007).

[3] R. P. Feynman, Phys. Rev. **56**, 340 (1939).

[4] P. Hohenberg and W. Kohn, Phys. Rev. **136**, 864 (1964).

[5] W. Kohn and L. J. Sham, Phys. Rev. A **140**, 1133 (1965).

[6] P. A. M. Dirac, Proc. Cambridge Phil. Soc. **26**, 376 (1930).

[7] E. P. Wigner, Trans. Faraday Soc. **34**, 678 (1938).

[8] J. Kohanoff, Electronic Structure Calculations for Solids and Molecules, Cambridge University Press, Cambridge (2006), ISBN:13-978-0-521-81591-8.

[9] R. M. Martin, Electronic Structure, Basic Theory and Practical Methods, Cambridge University Press, Cambridge (2004), ISBN: 978-0-521-78285-6.

[10] J. C. Slater, Phys. Rev. B **51**, 846 (1937).

[11] C. Herring, Phys. Rev. **57**, 1169 (1940).

[12] J. C. Philips and L. Kleinman, Phys. Rev. **116**, 287 (1959).

[13] D. R. Hamann, M. Schlüter, C. Chiang, Phys. Rev. Lett. **43**, 1494 (1979).

[14] D. Vanderbilt, Phys. Rev. B **41**, 7892 (1990).

[15] R. Pick, M. H. Cohen and R. M. Martin, Phys. Rev. B **1**, 910 (1970).

[16] S. Baroni, P. Giannozzi and A. Testa, Phys. Rev. Lett. **58**, 1861 (1987).

[17] S. Baroni, P. Giannozzi and A. Testa, Phys. Rev. Lett. **59**, 2662 (1987).

Chapter 3

Prediction of electronic topological transition in Sb_2Se_3*

3.1 Introduction

The search for three dimensional topological insulators (TI), a novel quantum state of matter, continues to persist among the materials scientists as it possesses potential importance in many technological applications like spintronics, quantum computation [1–3] because of the fact that the surface of such materials have polarized spins which exhibit spin-locking behavior, the result of which is helical spin arrangement on the surface. The direction of propagation of these spins on the surface of topological insulator is strongly dependent on their orientation [4–6] and can be manipulated in various ways

*Most of the works presented in this chapter has been published in Phys. Rev. Lett.: Achintya Bera, Koushik Pal, D. V. S. Muthu, Somaditya Sen, Prasenjit Guptasarma, Umesh V. Waghmare and Ajay K. Sood, **110**, 107401 (2013).

e.g. with photons [7] for practical applications. Recent study on topological insulators have drawn more attentions because of the proposed elusive particle-Majorana fermion, the manipulation of which may become the epitome for quantum computation [4,8] In condensed matter physics every phase of a material is associated with spontaneous broken symmetry of the system but topological insulator is a novel state of matter in the sense that it possesses topologically protected non-trivial phase even in the absence of any spontaneous symmetry breaking.

Topological insulators are a new class of insulators with topologically nontrivial electronic structure exhibiting a band gap in their bulk form [4,9]. The nontrivial topology of the electronic structure of bulk has interesting consequences to electronic states on their surfaces; for example, one-dimensional edge spin states in 2-dimensional quantum spin Hall systems. When a 3-dimensional TI is invariant under time reversal [5, 10], they exhibit gap less surface states that are robust because no time reversal symmetric perturbing potential can open up a gap at the surface. The nontrivial topology of electronic structure also gives rise to an intrinsic magneto-electric coupling through orbital magnetic polarization [11–13] and is expected to give rise to interesting and measurable response of a bulk TI. Topological insulators are characterized by topological invariants [4, 14], which are determined from the geometric properties of their electronic states as a function of Blöch vector. This links them naturally to the theory of electric polarization based on geometric or Berry phases Polarization, expressed as geometric phase, is non-unique and can be determined only within the ambiguity of an integer quantum polarization [15] associated with transport of an electronic charge

across the unit cell of the crystal. This quantum change in polarization can be shown to arise from a cyclic evolution of the insulator along a path that encloses a metallic state [16, 17]. Thus, nontrivial topology of electronic structure is intimately linked with the presence of a metallic state, which is expected to be relevant to an electronic topological transition (ETT).

Among all other binary semiconductors, Bi_2Se_3, Bi_2Te_3 and Sb_2Te_3 are predicted to be topological insulators whether Sb_2Se_3 is said to be a band insulator [5, 10].

Though in recent years, many topological insulators have been extensively studied both theoretically [5,10] and experimentally [18–21], a detailed pressure dependent study of electronic and vibrational properties is quite sparse [22]. Here we present bulk and surface electronic structures along with bulk vibrational properties of Sb_2Se_3 as a function of pressure and reveal that there exists an interesting electronic phase transition in Sb_2Se_3. By examining the band inversion of the highest occupied molecular orbital (HOMO) and lowest unoccupied molecular orbital (LUMO) at the Γ point in the Brillouin zone, we predict that Sb_2Se_3 undergoes ETT from band to topological insulator at $P_c = 2\ GPa$. Though the change in electronic topology in the bulk properties may be very subtle, the ETT in these materials can be concluded from closing-reopening of the gap *i.e.* band inversion and parity reversal [6, 8, 10] of the bulk wave function at the time reversal invariant momenta (TRIM) point of the bulk Brillouin zone.

3.2 Crystal structure

All materials of type A_2B_3 with $(A = Sb, Bi; B = Se, Te)$ has a layered rhombohedral structure in the bulk having space group $R\bar{3}m$ with D^5_{3d} crystal symmetry [5, 11]. The bulk unit cell has five atoms with $B(1) - A - B(2) - A - B(1)$ atomic plane arrangement along the $\langle 111 \rangle$ direction which is the closed packed direction for this crystal structure (see Fig. A.2). These five atomic layers make a quintuple layer (see Appendix A) which is stacked one-by-one along z-axis to create a layered structure. Among the five atoms in the unit cell, there are two inequivalent atoms-$B(1)$ and $B(2)$ which occupy the outermost and the third (central) layer in a quintuple layer (see Fig. A.3). The third $B(2)$ atom acts as the inversion center in the crystal unit cell. The crystal structure of A_2B_3 family of compounds can be cast into hexagonal form (see Fig. 3.1) which comprises of quintuple layers (QLs) stacked along the c-direction. Usually the semi-infinite surface of those materials consisting of three QLs are required in the surface unit cell to get a metallic surface state. [5] In our calculations we take three QLs in the surface unit cell unless otherwise specified.

3.3 Electronic structure methods

We use density functional theory based *first-principles* technique as implemented within the QUANTUM ESPRESSO (QE) code [23]. We adopt fully relativistic norm-conserving pseudopotentials to represent the interaction between the frozen core and the valence electrons of an atom facilitating the

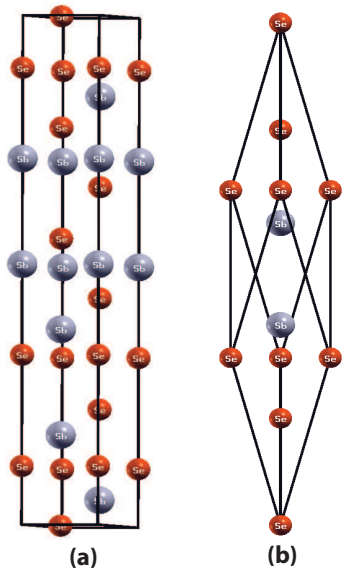

Figure 3.1: *Crystal structure of Sb_2Se_3 family of compounds for (a) surface and (b) bulk unit cell. The bulk rhombohedral unit cell consists of five atoms in $A(Se1)-B(Sb)-C(Se2)-A(Sb)-B(Se1)-C(Se1)$... arrangement along the z-direction. $Se2$ acts as the inversion center. The hexagonal supercell contains three quintuple layers stacked along c-axis. As each QL contains five atomic plane, the semi-infinite surface as shown in (b) contains total fifteen atomic layers with the inter and intra-quintuple layer distances being different.*

inclusion of spin-orbit coupling through Dirac equation in all *ab-initio* calculations presented here. The generalized-gradient approximation (GGA) [24] to the exchange-correlation functional as prescribed by Perdew, Burke and Ernzerhof (PBE) [25] is used while constructing the pseudopotentials. Unless otherwise specified, the electronic wave functions are expanded in plane wave basis with a cut-off energy of 80 Ry and for the charge density, the cut-off energy is chosen to be 360 Ry. The integration and sampling of the Brillouin zone are performed according to the Monkhorst-Pack [26] scheme with a dense k-mesh of $9 \times 9 \times 9$ and $12 \times 12 \times 1$ for the bulk and surface unit cell respectively. Occupation numbers are treated according to the Fermi-Dirac

smearing method with a broadening of 0.003 Ry. At each pressure, the bulk unit cell is fully relaxed using the Broyden-Fletcher-Goldfarb-Shanno scheme while keeping the c/a ratio fixed at the experimental value and varying the lattice constant a. While constructing the unit cell for surface calculations, we take the bulk atomic coordinates as the relaxation of atoms on the surface are very small. The vibrational frequencies are determined using both the frozen-phonon and linear response techniques. The details of the parameters for surface calculations and vacuum thicknesses of the slabs are given in Table 3.1 & 3.2 where c is meant to be the thickness of the slab without the vacuum.

$Pressure\ (GPa)$	$a(\mathring{A})$	$c(\mathring{A})$	$Vacuum(\mathring{A})$
0	4.09	29.96	15
3.5	3.99	29.29	15
4.0	3.96	29.11	15
5.0	3.89	28.50	14
7.2	3.85	28.20	14

Table 3.1: *Lattice constants and vacuum thicknesses for the hexagonal supercells of Sb_2Se_3 used for surface state calculations at different pressures. c is the thickness of the unit cell without the vacuum.*

$No.\ of\ QL$	$plane\ wave(Ry)$	$charge\ density(Ry)$	$c(\mathring{A})$	$Vacuum(\mathring{A})$
3	60	300	29.11	15
4	60	300	36.00	18
5	80	360	45.00	22
6	80	360	55.00	28
7	80	360	66.00	34

Table 3.2: *Cut-off energies for plane wave and charge density are given along with the vacuum thicknesses for Sb_2Se_3 at $P = 4.0\ GPa$ ($a = 3.96\mathring{A}$) for different number of quintuple layers in the surface unit cell.*

3.4 Results and analysis

At ambient pressure Sb_2Se_3 is so far known to be a semiconducting material with a band gap of 0.13 eV and having the topology of a trivial band insulator. Here, we report that Sb_2Se_3 undergoes an electronic phase transition at $P_c = 2\ GPa$ from band insulator to a topological insulator which has non-trivial topology in its electronic structure.

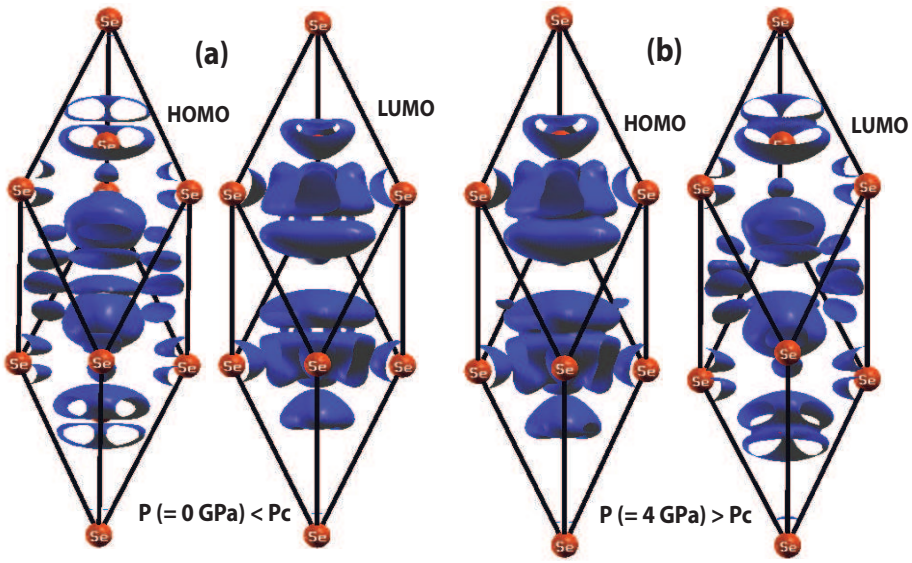

Figure 3.2: *Band inversion of Sb_2Se_3 across the critical pressure ($P_c = 2\ GPa$). Iso-surfaces of charge densities associated with the top of the valence (HOMO) and bottom of the conduction (LUMO) band at a pressure (a) before ($P = 0\ GPa$) and (b) after($P = 4\ GPa$) the critical pressure P_c.*

Our theoretical estimate of the lattice constant is $a = 4.09\mathring{A}$, at which a direct energy gap at the Γ point separates valence band states with odd parity from the conduction band states with even parity, as was shown by

Zhang et al. for a band insulator [5]. The odd parity of the state at the top of the valence band is evident in the involvement of the p orbitals of Se atoms present at the inversion center. A strong hybridization between p states of Sb and Se is evident in the electronic eigenstates across the gap (see Fig. 3.2). Band gap vanishes precisely at $P_c = 2\ GPa$ and opens up for $P > P_c$ with energies varying linearly with P near P_c . This involves an inversion of bands (see Fig. 3.2) and reversal of the parity (see Fig. 3.3) of valence and conduction bands across P_c marking a transition from a band insulator to a topological insulator.

As hydrostatic pressure is applied on the single crystal of Sb_2Se_3, the layers within the unit cell come closer to each other and thereby the interaction among themselves increases. This enhanced chemical interaction increases the strength of spin-orbit coupling between the central Se atoms and nearest Sb atoms which leads to inversion of HOMO (highest occupied molecular orbital) and LUMO (lowest unoccupied molecular orbital) across the transition pressure ($P_c = 2\ GPa$).

This increase in chemical interaction (strong hybridization between the p-orbitals of Sb and Se) can be noticed by visualizing the charge densities associated with the bands near the Fermi level around the critical pressure ($2\ GPa$) (see Fig.3.2). From the charge distributions of electronic states in Fig. 3.2, it is worth noting that intra-quintuple layer interaction or chemical bonding is stronger than inter-quintuple layer interaction in this layered material.

We use semi-infinite hexagonal supercell of Sb_2Se_3 containing three QLs

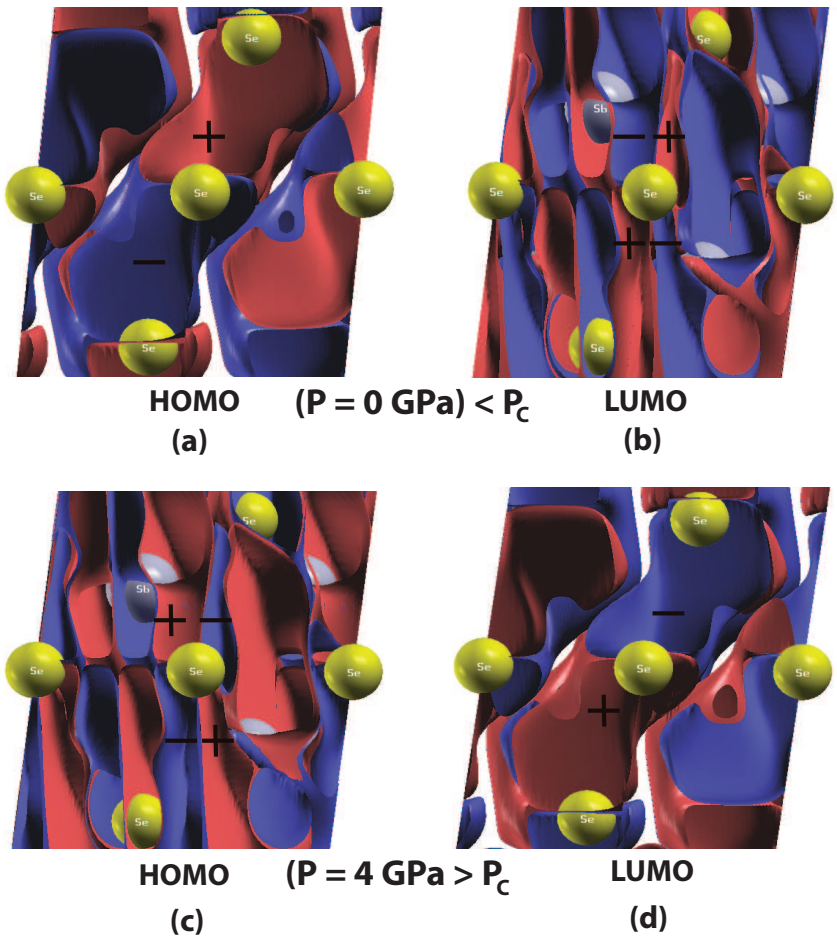

Figure 3.3: *Parity reversal of the bands of Sb_2Se_3 across the critical pressure (P_c = 2 GPa). Iso-surfaces of charge densities associated with the x-component of spinor wave function of valence (HOMO) and conduction (LUMO) band of Sb_2Se_3 having definite parities. HOMO of Sb_2Se_3 which has odd parity (Fig. 3.3a) at $P(0\ GPa) < P_c$ becomes of even parity (Fig. 3.3c)at $P(4\ GPa) > P_c$ and the LUMO of Sb_2Se_3 which has even parity (Fig.3.3 b) at $P(0\ GPa) < P_c$ becomes of odd parity (Fig. 3.3d) at $P(4\ GPa) > P_c$. The parities can be identified by the color of the orbitals involved in the above charge distributions. The middle layer of atoms in the above quintuple layer (see Fig. A.3 in Appendix A) i.e. $Se(2)$ atoms are at the inversion center of the unit cell as described in the text. Brown and blue colors represent positive and negative iso-surfaces of charge densities respectively (indicated with + and - signs in the figures)*

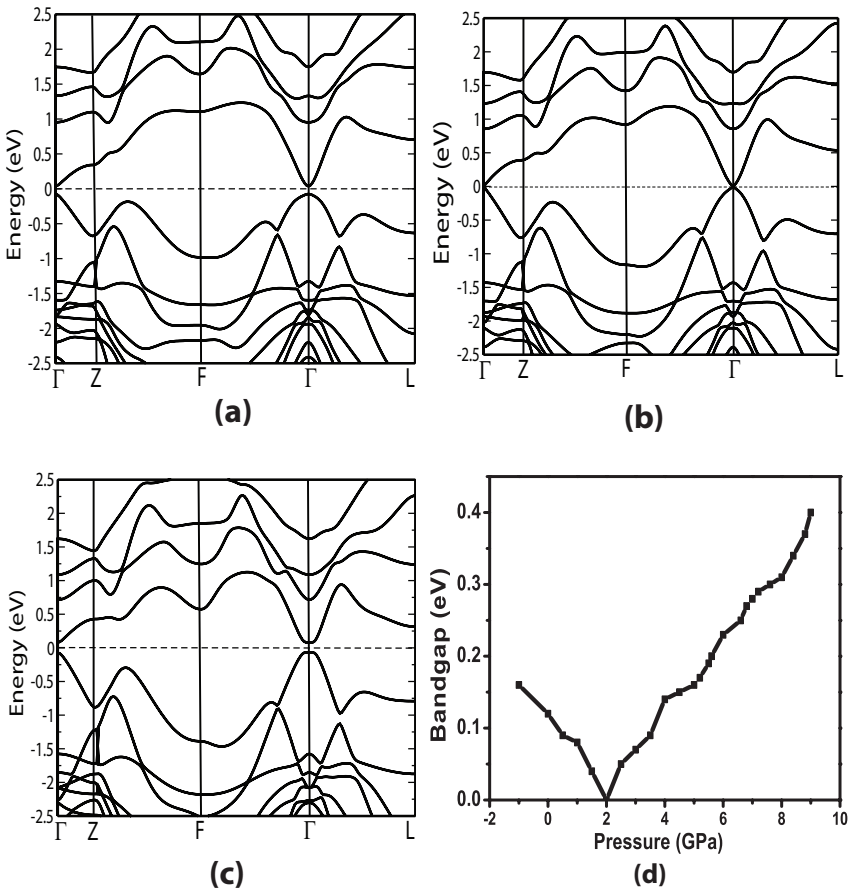

Figure 3.4: *Evolution of electronic bands and the bulk band gap near the critical pressure* $Pc(= 2\ GPa)$. *Electronic band structures of* Sb_2Se_3 *at (a)* $P(= 0\ GPa) < P_c$ *(b)* $P = Pc$ *and (c)* $P\ (= 4\ GPa) > P_c$.*(d) Closing and reopening of bulk band gap across the critical pressure causing the inversion of bands across* P_c.

for slab calculation and calculate the surface electronic structures as a function of pressure (see Fig. 3.5) which ranges from a point below P_c and extends above it. We found that there is a band gap in the surface electronic states below the critical pressure as anticipated. But to our surprise, above P_c the surface band gap does not close and no metallic state appears on the surface of Sb_2Se_3 in any of the TRIM points (see Fig. 3.5). One explanation behind

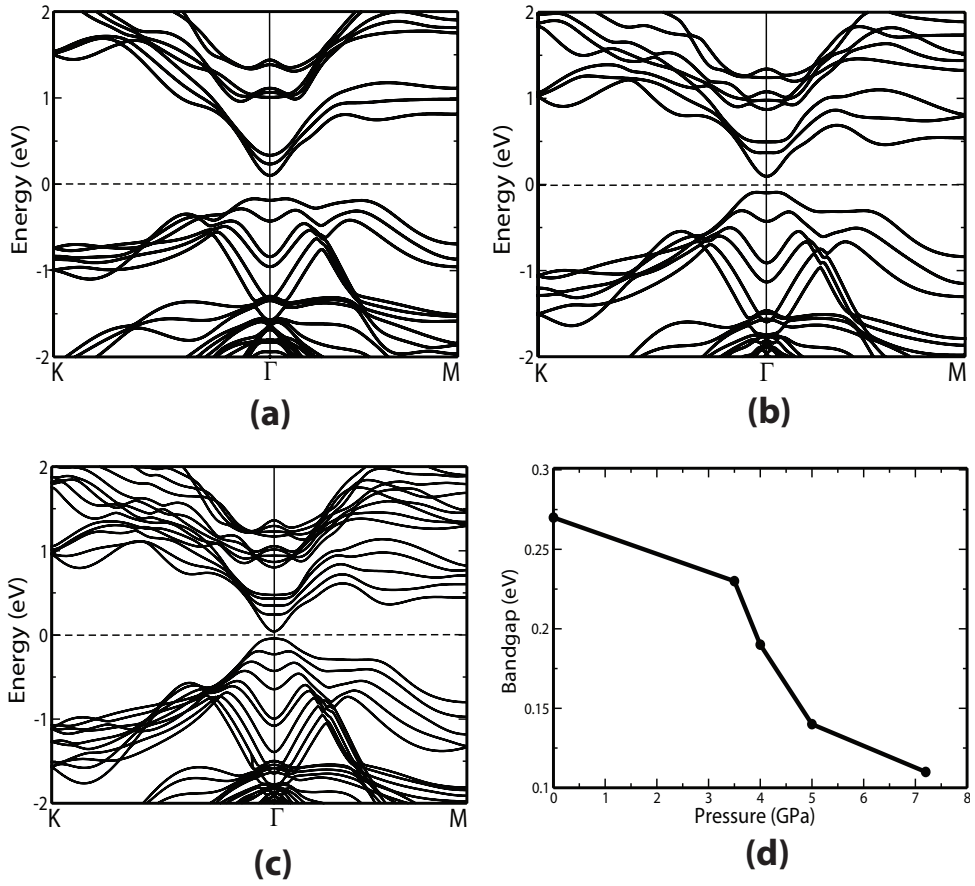

Figure 3.5: *Surface electronic structures of Sb_2Se_3 at different pressures and for different number of quintuple layers (QLs). (a) Surface states of Sb_2Se_3 before ($P = 0\ GPa$) and (b) after ($P = 4\ GPa$) the critical pressure (P_c) for 3-QL surface unit cell. Note that the surface band gap is not zero at $4\ GPa$ even if Sb_2Se_3 has entered into topological insulating phase. (c) Surface state of Sb_2Se_3 for 5-QL unit cell showing a reduced band gap than the 3-QL unit cell at $P = 4\ GPa$. (d) Surface band gap of 3-QL Sb_2Se_3 slab as a function of pressure.*

this behavior of the surface band gap could be the weak spin-orbit coupling interaction [11]. To increase the strength of the spin-orbit coupling, we increase the number of quintuple layers in the surface unit cell and examine the behavior of surface states upto seven QLs at a value of pressure ($P = 4GPa$)

which is above P_c. The dependency of surface band gap on quintuple layers is shown (see Fig. 3.6).

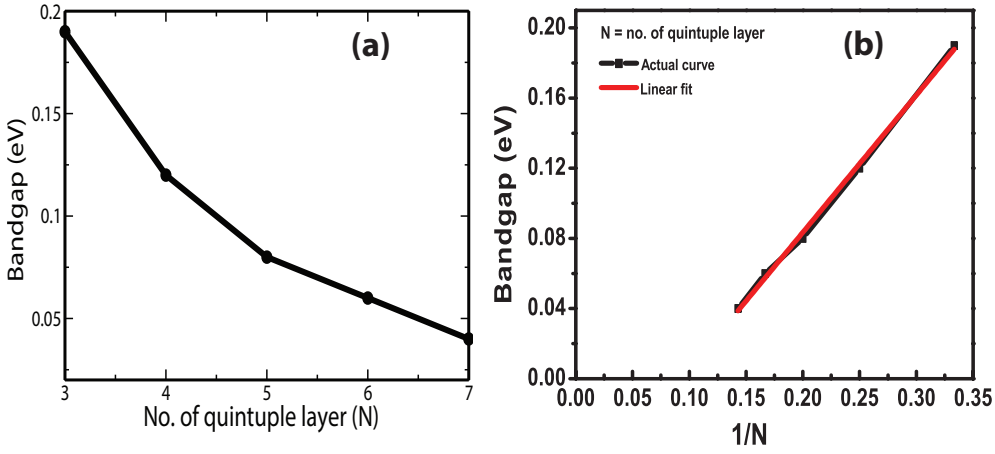

Figure 3.6: *Surface band gap of Sb_2Se_3 at 4 GPa for different slab thicknesses. (a) Dependency of surface band gap of Sb_2Se_3 on the number of quintuple layers (QLs) in the surface unit cell. (b) Surface band gap of Sb_2Se_3 plotted with inverse of the number of the QLs. The linear fit tells that the surface band gap should go to zero for eleven quintuple layers. Linear interpolation (not shown here) on the actual data points in the rightmost figure also predict that same number of QLs (i.e. eleven) are required to have a gapless surface state for Sb_2Se_3.*

We fit a linear curve (see Fig. 3.6 b) as well as performed linear interpolation technique on the actual data points of the QL-dependent surface band gap values which reveal that eleven quintuple layers are needed to have a gap-less surface state. This value of required quintuple layers is higher than what is reported in literature [11]. The detail investigation of the peculiar behavior of the surface states of Sb_2Se_3 is one of our future agendas.

Now we will discuss the vibrational properties of Sb_2Se_3 as a function of pressure. The bulk primitive unit cell for A_2B_3 type of compounds contain

five atoms. So according to group theory, the phonon modes of Sb_2Se_3 at the Γ point in the Brillouin zone are characterized by the irreducible representations of the rhombohedral point group D^5_{3d} *i.e.* fifteen vibrational modes which are given by, $2(A_{1g} + E_g) + 3(E_u + A_{2u})$. Among these modes, two E_{2u} and one A_{2u} modes are acoustic in nature whose frequencies are zero at the zone center and the rest twelve modes are non-zero optical modes. The displacement of the atoms in all optical modes vibration are shown in Fig. 3.8. In all the Raman active modes (A_{1g}, E_g), the displacement field involves the vibration of the two top most and two bottom most atomic planes within a quintuple layer while the middle layer which is at the inversion center remains fixed. In case of Infrared active (IR) modes (A_{2u}, E_u), all the atoms in a quintuple layer vibrate. The direction of atomic vibrations are longitudinal (along c-axis) for A_{1g}, A_{1u} modes, whereas the vibration of E_g, E_u modes occur in lateral direction (in ab-plane).

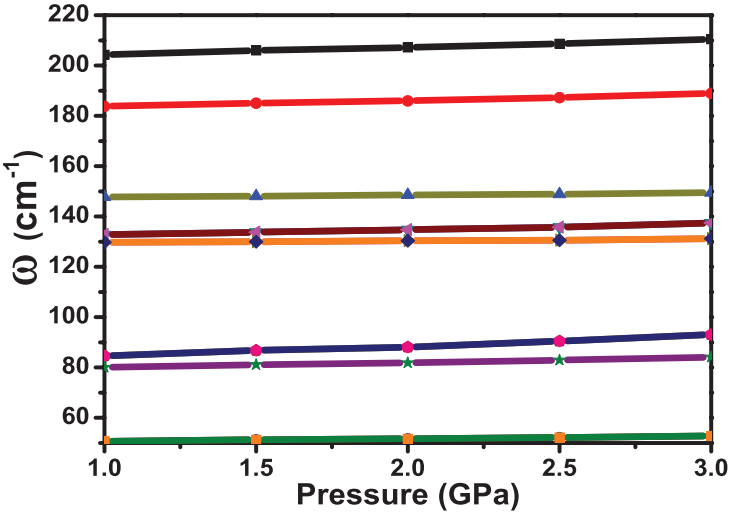

Figure 3.7: *Phonon frequencies of Sb_2Se_3 at the Γ point in the Brillouin zone. Frequencies of all the twelve optical modes vary linearly with pressure near $P_c(= 2\ GPa)$ showing no anomaly.*

The phonon frequencies are calculated with the help of two highly accurate techniques-linear response and frozen phonon method within the adiabatic density functional theory. Both the method yield phonon frequencies within few cm^{-1}. Phonon frequencies of Sb_2Se_3 vary linearly (see Fig. 3.7) with pressure at the Γ point in the Brillouin zone near P_c. The Nominal frequencies of Sb_2Se_3 are given and compared with other topological insulators in Table 3.3. From this table we can see that the frequencies for Sb_2Se_3 are higher than other componds because of the lighter masses of Sb and Se atoms as compared to Bi and Te atomic masses.

	A^2_{1g}	A^1_{1g}	E^2_g	E^1_g	A^2_{2u}	A^1_{2u}	E^2_u	E^1_u
[a] Sb_2Se_3	211.5	78	138.3	53.2	190.9	149.8	131.4	94.6
[18],[b] Sb_2Te_3	169	67	117	49	146	109	100	77
[19],[c] Sb_2Te_3	165	69	112					67
[20],[b] Bi_2Se_3	166.3	63.8	123.9	38.8	155.4	136.7	126.8	64.7
[21],[c] Bi_2Se_3	175.3	73.3	132.6	39.9	159.9	128.9	124.9	67.9
[20],[b] Bi_2Te_3	127.2	53.8	95.9	35.4	118.6	95	91.2	48.4
[22],[c] Bi_2Te_3	134.1	62.0	101.7	34.3				

[a] this work, [b] theoretical calculation and [c] experiment.

Table 3.3: *Vibrational frequencies of twelve optical modes* $2(A_{1g}+E_g+A_{2u}+E_u)$ *of topological insulator materials having* D^5_{3d} *crystal symmetry. All frequencies are in the unit of* cm^{-1} *The vibrational frequencies of* Sb_2Se_3 *are given here at* $P = 3.5\ GPa$ *in its topological insulating phase. For other materials which are already TI in ambient pressure, the above frequencies are at equilibrium lattice constant i.e at zero pressure. g and u denote Raman (R) and Infrared (IR) active modes respectively.*

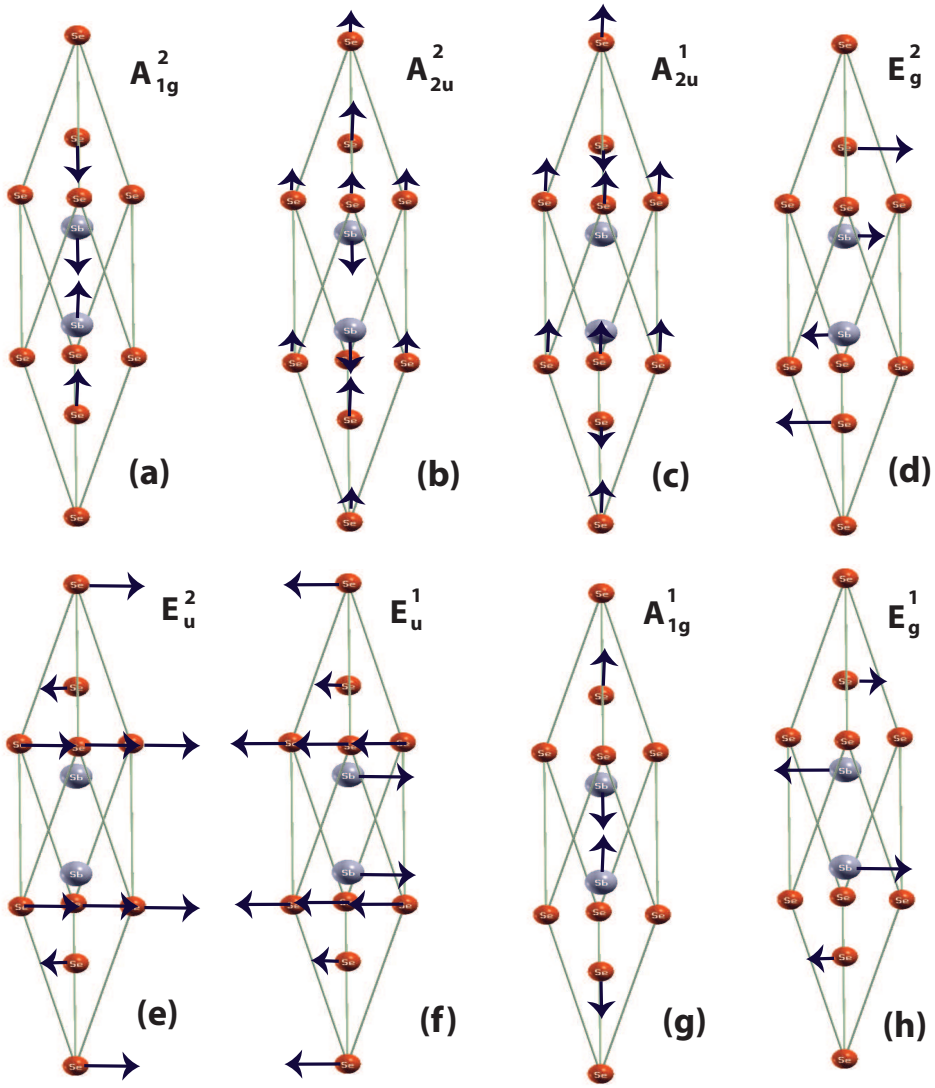

Figure 3.8: *Optical phonon modes of Sb_2Se_3. (a)-(c), (g) are singly degenerate . (d)-(f), (h) are doubly degenerate mode. A_{1g} and E_g are Raman active, A_{2u} and E_u are infrared active. Displacements of the atoms are in the direction of the arrowhead marked in the figures. Larger arrow signifies larger displacement of the atoms.*

3.5 Going beyond adiabatic approximation

As Sb_2Se_3 passes through the metallic state with zero bulk band gap at P_c, the time scale associated with the electronic motion near P_c becomes

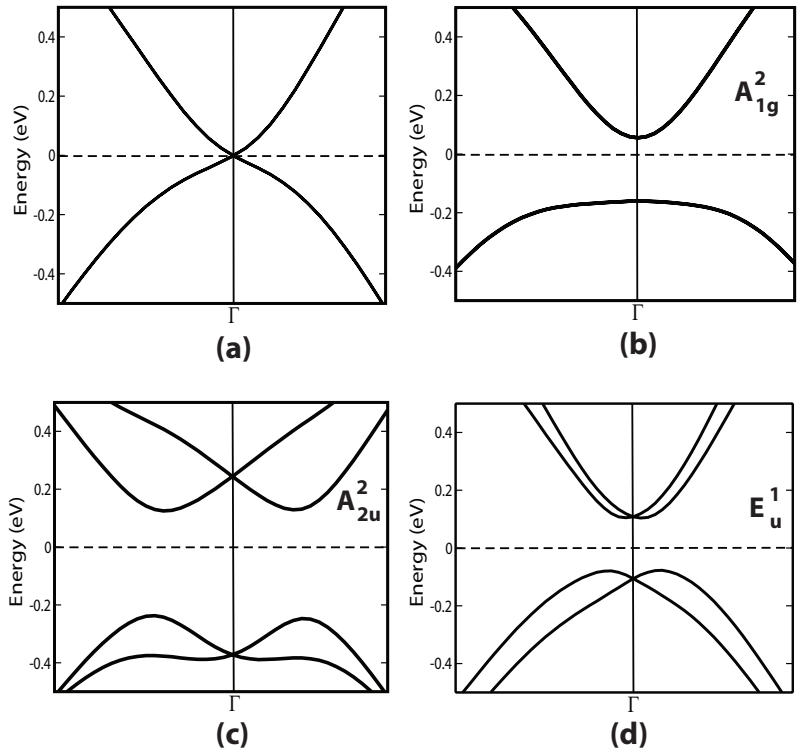

Figure 3.9: *(a) The electronic bands of Sb_2Se_3 at P_c near the Γ point for the undistorted crystal structure. First-principles evidence of electron-phonon coupling obtained by distorting the crystal structure along the direction of displacement of atoms for (b) A^2_{1g}, (c) A^2_{2u} and (d) E^1_u mode. The form of electron phonon coupling for A_{2u} mode (see text) yields splitting of bands near the gap obtained within the 4-band model, which has been verified using first-principles calculations. Evidence of electron-phonon coupling for rest of the phonon modes are presented in the Appendix B.*

comparable with that of the phonons and the adiabatic *Born-Oppenheimer* approximation may break down very close to the ETT at P_c and one may need to include dynamical corrections. Thus the resulting slow dynamics of the electron is expected to interact with the phonons giving rise to anomaly in vibrational frequencies.

But no anomaly is observed in vibrational frequencies as calculated within

DFT (Fig. 3.7). This suggests that the mean field behavior of the vibrational frequencies near the transition pressure (P_c) are beyond the adiabatic description of density functional theory [27]. Thus investigations of phonon anomaly near P_c requires going beyond the adiabatic approximation.

An occurrence of broken adiabaticity has been seen in graphene, also characterized by a vanishing band gap: explanation of vibrational signatures of doping in graphene probed by Raman spectroscopy required going beyond the *Born-Oppenheimer* (adiabatic) approximation [28, 29].

We now present theoretical analysis beyond the adiabatic approximation and determine dynamical [28, 29] corrections to phonon frequencies to understand the observed Raman anomalies as seen in experiment by our collaborators [27]. To this end, we build on the universal four band model developed by Zhang et al. [5, 30] written in terms of Dirac matrices. To capture the pressure dependence of electronic structure in the neighborhood of P_c (see Fig. 3.9), we note that states at the top of the valence and bottom of the conduction bands are doubly degenerate, and their energies are given by $C_0 \pm M_0$, where C_0 and M_0 are the parameters of the model Hamiltonian [30], and $M_0 < 0$ for a topological insulator. Treating $M_0 = -\kappa(P - Pc)$ with a positive κ, we reproduce the electronic structure near the Γ point close to the transition from a band insulator to a topological insulator (see Fig. 3.9) as reflected in the reversal of bands of opposite parity. Electron-phonon coupling is needed to estimate dynamical corrections to vibrational frequencies, and we now derive their form at the lowest order within the four-band model, expressing them in terms of Dirac matrices (see Appendix E for a discussion on Dirac matrices). Symmetry properties of the Dirac matrices (irreducible

representations for the symmetry group of Sb_2Se_3) have been derived by Liu et al. [30]. We note that Raman-active and IR-active modes have even and odd parity, all of them are invariant under time reversal. An electron-phonon coupling term in the Hamiltonian can be expressed as a product of phonon degree of freedom and a Dirac matrix (or its commutator)(see Appendix C for a detailed discussion). A symmetry-invariant electron-phonon coupling is obtained by projecting this term onto identity representation of the double group of D_{3d}^5. For the Raman-active A_{1g}^2 mode, which has the full symmetry of the system, the electron-phonon coupling can have all the terms in the four-band electronic Hamiltonian multiplied by the mode displacement $u_{A_{1g}}$. We pick the leading term that gives changes in band structure obtained by distorting the structure with this mode (see Fig. 3.9 b):

$$H_{A_{1g}} = A_{A_{1g}} u_{A_{1g}} \Gamma_5, \tag{3.1}$$

where Γ_5 is a Dirac matrix. Similarly, coupling of an IR-active mode A_{2u}^2 with electrons takes a form:

$$H_{A_{2u}} = A_{A_{2u}} u_{A_{2u}} \Gamma_{45}, \tag{3.2}$$

where Γ_{ij} is a Dirac matrix commutator $[\Gamma_i, \Gamma_j]/2i$. Finally, symmetry consideration of the lowest order coupling of the E_g^2 mode with electrons requires one to have a quadratic form of Dirac matrices:

$$H_{E_g} = A_{E_g}(u_{E_g}^x \Gamma_{15} + u_{E_g}^y \Gamma_{25})\Gamma_{35}, \tag{3.3}$$

where x and y denote Cartesian components of displacements of the doubly degenerate E_g^2 mode. In this term, each of matrix Γ_{35} and the expression $u^x_{E_g}\Gamma_{15} + u^y_{E_g}\Gamma_{25}$ transform according to Γ_1^- irrep and is even under time reversal, and their product is symmetry-invariant. Since the product of two non-commuting Hermitian operators is not Hermitian, we construct a symmetry-invariant Hermitian form:

$$H_{E_g} = A_{E_g}[(u^x_{E_g}\Gamma_{15} + u^y_{E_g}\Gamma_{25})\Gamma_{35} - H.c.]/2i, \tag{3.4}$$

where H.c. means Hermitian conjugate. Similarly, there are other forms of electron and E_g^2 phonon couplings possible:

$$B_{E_g}[(u^x_{E_g}\Gamma_{24} - u^y_{E_g}\Gamma_{14})\Gamma_{34} - H.c.]/2i + B'_{E_g}[(u^x_{E_g}\Gamma_{24} - u^y_{E_g}\Gamma_{14})\Gamma_{12} - H.c.]/2i$$
$$+C_{E_g}(k_x u^x_{E_g} - k_y u^y_{E_g})\Gamma_4,$$

where the term with coupling B and B$'$ (C) involves products of Γ_2^+ (Γ_2^-) representations, each of which is odd under time-reversal.

We validate the form of electron-phonon coupling by comparing the electronic structure of the model with that obtained from first-principles for the lattice distorted with each mode of Sb_2Se_3 (see Fig. 3.9) for the case of A^2_{2u} and A^2_{1g} modes). For a frozen A^2_{1g} mode at $P = P_c$, band gap opens up in a way similar to how it opens up at infinitesimally small deviation in pressure or strain. For a frozen A^2_{2u} mode, band splitting is more interesting: each of the doubly degenerate valence and conduction bands of definite parity split up as this mode breaks the parity symmetry. The minima or maxima of bands shift away from the Γ point. However, the splitting or changes

in the model band structure associated with the electron-phonon coupling of E_g^2 (A_{E_g}) mode are not captured within first-principles calculations (see the figures in Appendix B), suggesting that the physics of this coupling is beyond the formal mean-field description of density functional theory used here. Thus, in the analysis below, we use the symmetry invariant form with A-coupling as a free parameter as the other terms are not needed to capture the essential aspects of the observed phonon anomalies.

We obtain the dynamical corrections to phonon frequencies as a function of pressure using these forms of electron-phonon couplings (keeping strength of the coupling as free parameters) in first-order time dependent perturbation analysis [28] (see Appendix D) of the four-band model of Bi_2Se_3 derived by Zhang et al. [5] with pressure dependent M_0 (see Fig. 3.10). To simplify our analysis, we make use of the layered nature of Sb_2Se_3 and carry out Brillouin zone integrations only in the *ab*-plane. It is evident that dynamical corrections to frequencies of Raman active modes change sharply below P_c and asymmetrically around P_c. Indeed, the sharp drop (see Fig. 3.10) in frequencies of E_g^2 and A_{1g}^2 modes just below P_c, and a gradual increase in their frequencies for $P > P_c$ are consistent with the pressure-dependent behavior of the modes seen in experiment [27]. In contrast, dynamical corrections to IR-active mode exhibit a sharp jump above P_c!

The line-width *i.e* FWHM (full width at half maximum) of E_g^2 mode estimated from our analysis (see Fig.3.10d and Eq.(D.4) of Appendix D) peaks *asymmetrically* near the transition pressure, quite consistent with the observed line-width anomaly seen in experiments [27]. This further corroborates our theoretical analysis, and allows us to determine the origin of

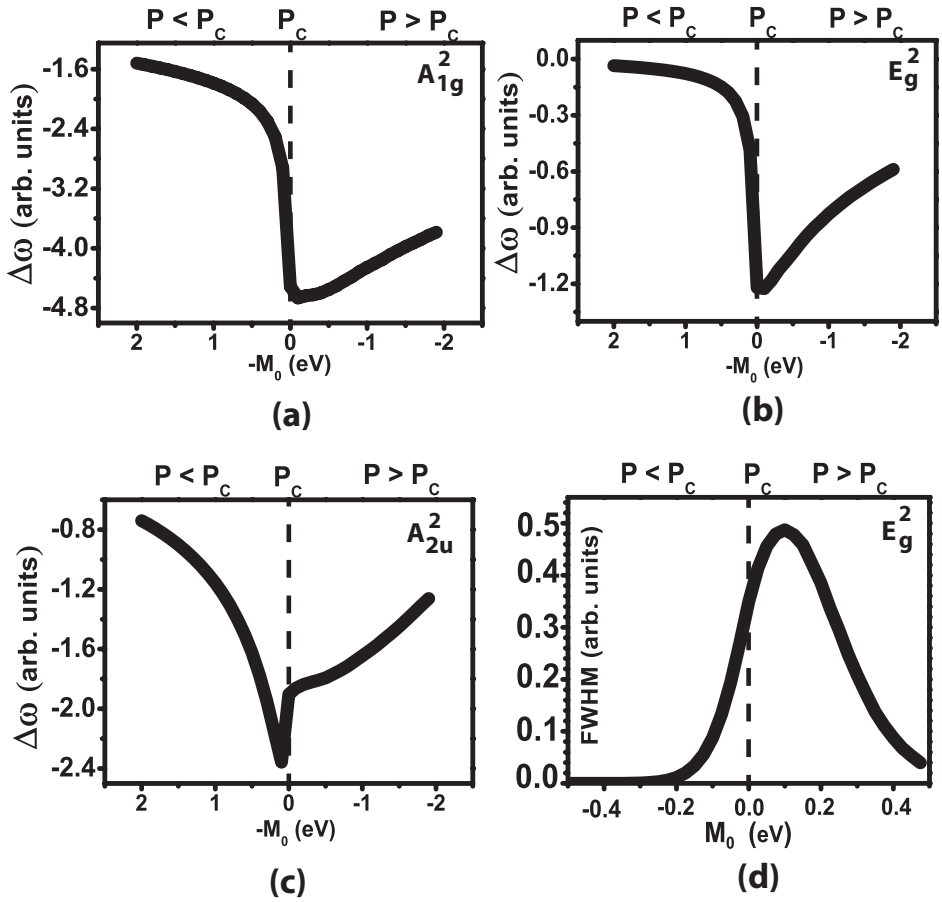

Figure 3.10: *Dynamical corrections to frequencies of phonon modes (a) A^2_{1g}, (c) E^2_g and (c) A^2_{2u} as a function of $-M_0$ (i.e. $\propto (P - P_c)$). The corrections are negative and make the modes softer near the transition; their asymmetry allows differentiation between the trivial and the nontrivial topology of electronic structure on the two sides of the transition. Fig.3.9 show how electronic structure changes when atomic displacements of a given phonon mode are frozen to distort the structure based on first-principles calculations, and are reproduced using electron-phonon coupling (see text) within the 4-band model. (d) The calculated linewidth (FWHM) of the mode E^2_g as a function of M_0 i.e. pressure.*

asymmetry in phonon anomalies. It can be traced to the parity reversal of occupied and unoccupied bands in immediate vicinity of the ETT. Using the form of electron-phonon coupling for the IR-active mode in perturbative

analysis, we predict that (i) dynamical corrections should lead to anomalies in IR-spectra of Sb_2Se_3 in narrow neighborhood of the transition pressure P_c, and (ii) the asymmetry in anomaly of the IR-active mode will be in contrast to that in the Raman mode–with a jump in frequency above P_c.

3.6 Conclusion

In conclusion, we reveal a pressure-induced electronic topological transition (ETT) in single crystal of Sb_2Se_3, a band insulator. A combination of first-principles calculations and theoretical model-based analysis presented here show a breakdown of adiabatic approximation at the ETT. We established that electron-phonon coupling of nontrivial forms leads to anomalies as observed in the experimental Raman spectra [27]. These ideas are applicable to electronic transitions in other topological insulators too, and expected to stimulate experiments for exploring anomalies in IR vibrational spectra, and guide materials scientists in transforming a normal insulating materials to a topological insulator.

Bibliography

[1] L. Fu and C. L. Kane, Phys. Rev. Lett. **100**, 096407 (2008).

[2] A. R. Akhmerov, J. Nilsson and C. W. J. Beenakker, Phys. Rev. Lett. **102**, 216404 (2009).

[3] K. T. Law, P. A. Lee and T. K. Ng, Phys. Rev. Lett. **103**, 237001 (2009).

[4] L. Fu, C. L. Kane and E. J. Mele, Phys. Rev. Lett. **98**, 106803 (2007).

[5] H. Zhang, C. X. Liu, X. L. Qi, X. Dai, Z. Fang and S. C. Zhang, Nature Physics **5**, 438 (2009).

[6] B. A. Bernevig, T. L. Hughes and S. C. Zhang, Science **314**, 1757 (2006).

[7] C. Jozwiak, C. H. Park, K. Gotlieb, C. Hwang, D. H. Lee, S. G. Louie, J. D. Denlinger, C. R. Rotundu, R. J. Birgeneau, Z. Hussain and A. Lanzara, Nature Physics doi:10.1038/nphys2572 (2013) (in press).

[8] X. L. Qi and S. C. Zhang, Rev. Mod. Phys. **83**, 1057 (2011).

[9] C. L.Kane and E. J. Mele, Phys. Rev. Lett. **95**, 146802 (2005).

[10] W. Zhang, R. Yu, H. Zhang, X. Dai and Z. Fang, New Journal of Physics **12**, 065013 (2010).

[11] W. Liu, X. Peng, C. Tang, L. Sun, K. Zhang and J. Zhong, Phys. Rev. B **84**, 245105 (2011).

[12] A. Essin, J. E. Moore and D. Vanderbilt, Phys. Rev. Lett. **102**, 146805 (2009).

[13] A. Essin, A. M. Turner, J.E. Moore and D. Vanderbilt, Phys. Rev. B **81**, 205104 (2010).

[14] J. E. Moore, Nature(London) **464**, 194 (2010).

[15] R. D. King-Smith and D. Vanderbilt, Phys. Rev. B **47**, 1651(R) (1993).

[16] U. V. Waghmare, Ph.D. thesis, Yale University (1996).

[17] K. M. Rabe and U. V. Waghmare, Ferroelectrics **136**, 147 (1992).

[18] Y. L. Chen, J. G. Analytis, J. H. Chu, Z. K. Liu, S. K. Mo, X. L. Qi, H. J. Zhang, D. H. Lu, X. Dai, Z. Fang, S. C. Zhang, I. R. Fisher, Z. Hussain and Z. X. Shen, Science **325**, 178 (2009).

[19] Y. Xia, D. Qian, D. Hsieh, L. Wray, A. Pal, H. Lin, A. Bansil, D. Grauer, Y. S. Hor, R. J. Cava and M. Z. Hasan, Nature Physics **5**, 398 (2009).

[20] D. Hseish, Y. Xia, D. Qian, L. Wray, F. Meier, J. H. Dil, J. Osterwalder, L. Patthey, A. V. Fedorov, H. Lin, A. Bansil, D. Grauer, Y. S. Hor, R. J. Cava and M. Z. Hasan, Phys. Rev. Lett. **103**, 146401 (2009).

[21] K. Kuroda, M. Arita, K. Miyamoto, M. Ye, J. Jiang, A. Kimura, E. E. Krasovskii, E. V. Chulkov, H. Iwasawa, T. Okuda, K. Shimada, Y. Ueda, H. Namatame and M. Taniguchi, Phys. Rev. Lett. **105**, 076802 (2010).

[22] R. Vilapana, D. Santamara-Prez, O. Gomis, F. J. Manjn, J. Gonzlez, A. Segura, A. Muoz, P. Rodrguez-Hernndez, E. Prez-Gonzlez, V. Marn-Borrs, V. Muoz-Sanjose, C. Drasar and V. Kucek, Phys. Rev. B **84**, 184110 (2011).

[23] QUANTUM-ESPRESSO is a community project for high-quality quantum-simulation software, based on density-functional theory, and coordinated by P. Giannozzi. See `http://www.quantum-espresso.org` and `http://www.pwscf.org`.

[24] X. Hua, X. Chen and W. A. Goddard III, Phys. Rev. B **55**, 16103 (1997).

[25] J. P. Perdew, K. Burke and M. Ernzerhof, Phys. Rev. Lett. **77**, 3865 (1996).

[26] H. Monkhorst and J. D. Pack, Phys. Rev. B **13**, 5188 (1976).

[27] A. Bera, K. Pal, D. V. S. Muthu, S. Sen, P. Guptasarma, U. V. Waghmare and A. K. Sood, Phys. Rev. Lett. **110**, 107401 (2013).

[28] S. Pisana, M. Lazzeri, C. Casiraghi, K. S. Novoselov, A. K. Geim, A. C. Ferrari and F. Mauri, Nature Materials **6**, 198 (2007).

[29] A. Das, S. Pisana, B. Chakraborty, S. Piscanec, S. K. Saha, U. V. Waghmare, K. S. Novoselov, H. R. Krishnamurthy, A. K. Geim, A. C. Ferrari and A. K. Sood, Nat. Nanotechnol. **3**, 210 (2008).

[30] C. X. Liu, X. L. Qi, H. J. Zhang, X. Dai, Z. Fang and S. C. Zhang, Phys. Rev. B **82**, 045122 (2010).

Appendices

Appendix A

Structural relationship between the rhombohedral and hexagonal cell of Sb_2Se_3

Among all three closed packed crystal systems (trigonal, hexagonal and cubic), crystal structures belonging to the the trigonal class can have either rhombohedral lattice or hexagonal lattice. Primitive unit cell of hexagonal lattice has $a = b \neq c; \alpha = \beta = 90^\circ \neq \gamma = 120^\circ$ and for the rhombohedral unit cell $a = b = c; \alpha = \beta = \gamma \neq 90^\circ$. Both the lattice can be referred to either the rhombohedral or the hexagonal axes. When a rhombohedral lattice is specified by hexagonal axes, then the hexagonal cell becomes non-primitive and the *vice versa*. In Fig. A.1 the primitive unit cell is the rhombohedral one with lattice constants ($\mathbf{a} = \mathbf{b} = \mathbf{c}$) and the hexagonal cell being the non-primitive ($\mathbf{a_1} = \mathbf{b_1} \neq \mathbf{c_1}$). Unit cell vectors of a rhombohedral cell can be listed with hexagonal lattice constants as follows,

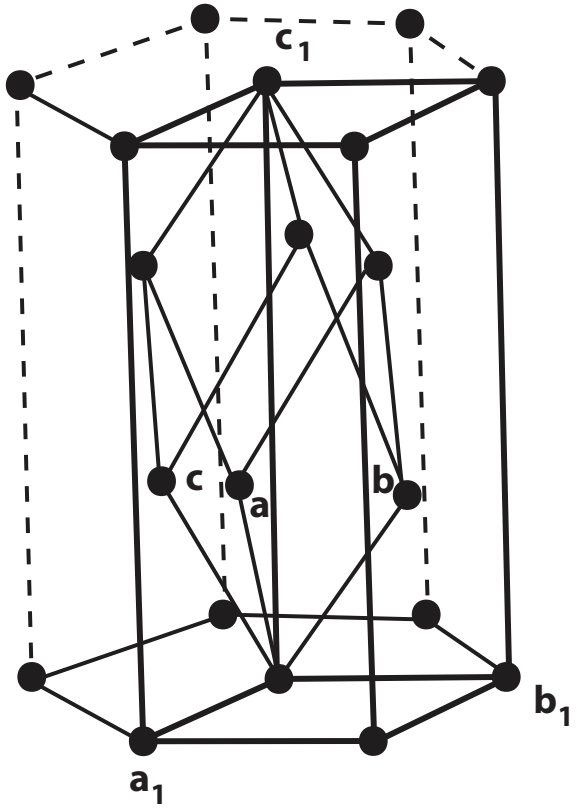

Figure A.1: *Relation between the hexagonal and rhombohedral crystal structures shown in a prototype crystal cell. Unit cell of rhombohedral lattice with lattice constants* $(\mathbf{a}, \mathbf{b}, \mathbf{c})$ *and the corresponding hexagonal crystal structure with* $(\mathbf{a_1}, \mathbf{b_1}, \mathbf{c_1})$ *lattice parameters are shown here. The hexagonal lattice is highlighted in bold lines.*

$$\begin{cases} \vec{\mathbf{r_1}} = (1/2\ \mathbf{a_1}, 1/\sqrt{12}\ \mathbf{a_1}, 1/3\ \mathbf{c_1}) \\ \vec{\mathbf{r_2}} = (1/\sqrt{3}\ \mathbf{a_1}, 0, 1/3\ \mathbf{c_1}) \\ \vec{\mathbf{r_3}} = (-1/2\ \mathbf{a_1}, -1/\sqrt{12}\ \mathbf{a_1}, 1/3\ \mathbf{c_1}) \end{cases} \tag{A.1}$$

The relations between the hexagonal and rhombohedral lattice constants are given by,

$$\begin{cases} \mathbf{a_1} = 2\mathbf{a}\ Sin(\theta/2) \\ \mathbf{c_1} = \mathbf{a}[3\{1 + 2Cos(\theta/2)\}]^{1/2} \end{cases} \tag{A.2}$$

The hexagonal unit cell of a rhombohedral lattice which has n layers, is made up of three elementary stacking of $n/3$ layers that are related to each other either by anti-cyclic shift ($A \rightarrow C \rightarrow B \rightarrow A$) or cyclic shift ($A \rightarrow B \rightarrow C \rightarrow A$).

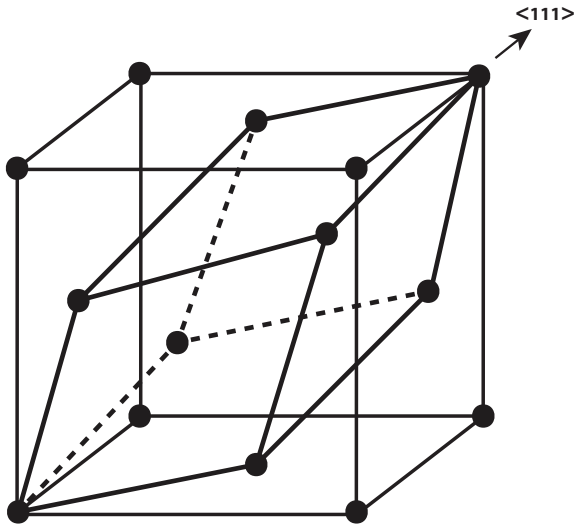

Figure A.2: *Schematic demonstration of how the closed packed direction of the rhombohedral unit cell coincides with the* $\langle 111 \rangle$*-direction of the fcc unit cell.*

The relationship between the face centered cubic (fcc) and the primitive rhombohedral unit cell is shown in Fig. A2. The trigonal axis of the rhombohedral unit cell coincides with one of the $\langle 111 \rangle$ directions of the cubic unit cell and thus the layers are stacked along $\{111\}$ planes in the cubic closed packing.

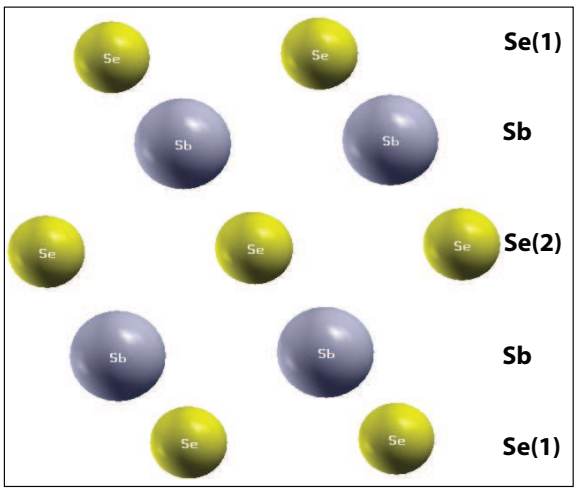

Figure A.3: *Layered structure of Sb_2Se_3. A quintuple layer with $Se(1)-Sb-Se(2)-Sb-Se(1)$ atomic plane arrangements is indicated within the box. The middle layer i.e. $Se(2)$ atoms are at the inversion center.The smaller sphere (yellow) and larger sphere (grey) denote Se and Sb atoms respectively*

A quintuple layer of Sb_2Se_3 is shown in Fig. A.3, where the layers orient themselves in $A(Se1) \rightarrow B(Sb) \rightarrow C(Se2) \rightarrow A(Sb) \rightarrow B(Se1) \rightarrow C(Se1)$ fashion as discussed above. The middle layer (*i.e.* $Se(2)$) is at the inversion centre of the quintuple layer.

Bibliography

[1] International Tables for Crystallography, Vol. A, Springer, Dordrecht (2005).

[2] International Tables for Crystallography, Vol. C, Kluwer Academic Publishers, Dordrecht (2004).

[3] http://cst-www.nrl-navy.mil/lattice/struk/c33.html.

Appendix B

Electron-phonon coupling from first-principles

To see how the topology of electronic band changes due to electron-phonon coupling, we distort the equilibrium crystal structure of Sb_2Se_3 at $P = P_c$ with the corresponding mode displacement vectors and calculate the electronic band structure for each mode.

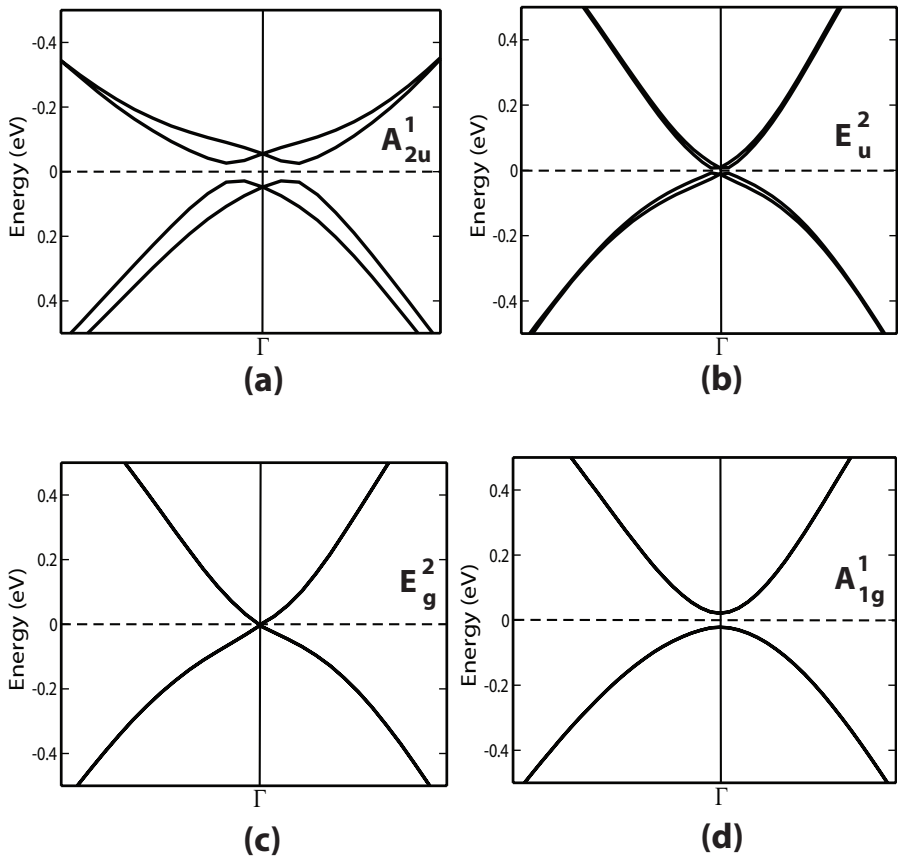

Figure B.1: *Change in electronic structure of Sb_2Se_3 due to electron-phonon coupling for (a) A^1_{2u} (b) E^2_u (c) E^2_g and (d) A^1_{1g} vibrational mode as calculated within the density functional theory.*

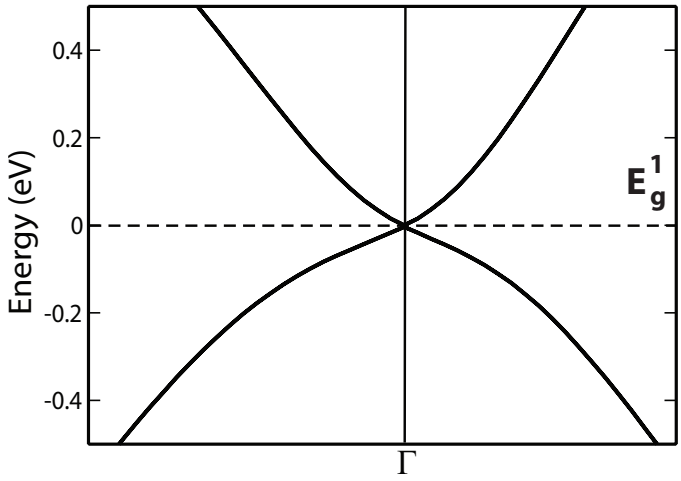

Figure B.2: *Form of electron-phonon coupling as obtained with DFT calculation for the E_g^1 mode of Sb_2Se_3 showing no change in the electronic band structure.*

Appendix C

Electron-phonon coupling Hamiltonian

We now derive the electron-phonon coupling (EPC) Hamiltonian using projection operator technique. Projection operator [1] can be written as $\hat{\mathbf{P}}_{\tilde{\Gamma}_n^{\pm}} = \frac{1}{g}\sum_{\mathcal{R}} A_{\tilde{\Gamma}_n^{\pm}}(\mathcal{R})\hat{P}_{\mathcal{R}}$, where $\hat{P}_{\mathcal{R}}$ is the symmetry operator corresponding to symmetry operation $\mathcal{R}$ and $A_{\tilde{\Gamma}_n^{\pm}}(\mathcal{R})$ is the character of $\tilde{\Gamma}_n^{\pm}$ irreducible representation (irrep) of the symmetry group and sum is over all the symmetry operations of the group (D_{3d}^5) and g is its order. $\pm$ sign represent even and odd parity respectively of the irreps. The phonon eigenmodes A_{1g}, A_{2u} and E_g have the symmetry of the irreducible representations given respectively by $\tilde{\Gamma}_1^+, \tilde{\Gamma}_2^-$ and $\tilde{\Gamma}_3^+$ [1]. We first considered direct product representation obtained from a multiplication of an irrep of a phonon mode and each irrep of D_{3d}^5. From these, we pick the ones that contain identity representation of D_{3d}^5. We write the electron-phonon coupling term by projecting the product

of the suitable Dirac matrix and u mode displacement onto identity representations [2]. For A_{1g} mode, picking only the leading terms which give significant change in band structure, the EPC Hamiltonian can be written as,

$$H_{A_{1g}} = \hat{\mathbf{P}}_{(\tilde{\Gamma}_1^+ \equiv A_{1g})}.[u_{A_{1g}}\Gamma_5] \simeq A_{A_{1g}} u_{A_{1g}}\Gamma_5 \tag{C.1}$$

Similarly for A_{2u} mode the EPC Hamiltonian is given by the following expression,

$$H_{A_{2u}} = \hat{\mathbf{P}}_{(\tilde{\Gamma}_2^- \equiv A_{2u})}.[u_{A_{2u}}\Gamma_5] \simeq A_{A_{2u}} u_{A_{2u}}\Gamma_{45}, \tag{C.2}$$

where we note that each of $u_{A_{2u}}$ and Γ_{45} belongs to $\tilde{\Gamma}_2^-$ irrep. Here Γ_m is a Dirac matrix and $u_{A_{1g}}$, $u_{A_{2u}}$ are the displacement of the A_{1g} and A_{2u} phonon modes respectively.

For E_g mode,

$$\hat{\mathbf{P}}_{(\tilde{\Gamma}_1^+)}.[\{u^x_{E_g}, u^y_{E_g}\} \otimes \{\Gamma_{15}, \Gamma_{25}\}].\Gamma_{35} \simeq A_{E_g}(u^x_{E_g}\Gamma_{15} + u^y_{E_g}\Gamma_{25})\Gamma_{35} \tag{C.3}$$

where $\Gamma_{mn} = [\Gamma_m, \Gamma_n]/2i$. $u^x_{E_g}$ and $u^y_{E_g}$ are the x and y component of the displacement of the E_g phonon mode. However, this form is not Hermitian and we construct a Hermitian operator with the same symmetry properties using:

$$H_{E_g} \simeq A_{E_g} \frac{(u^x_{E_g}\Gamma_{15} + u^y_{E_g}\Gamma_{25})\Gamma_{35} - H.c.}{2i}, \tag{C.4}$$

where $H.c.$ means Hermitian conjugate.

Similarly other symmetry allowed lowest order terms for EPC Hamiltonian of H_{E_g} mode are,

$$B_{E_g} \frac{(u^x_{E_g}\Gamma_{24} - u^y_{E_g}\Gamma_{14})\Gamma_{34} - H.c.}{2i} + B'_{E_g} \frac{(u^x_{E_g}\Gamma_{24} - u^y_{E_g}\Gamma_{14})\Gamma_{12} - H.c.}{2i} + C_{E_g}(k_x u^x_{E_g} - k_y u^y_{E_g})\Gamma_4 \tag{C.5}$$

Bibliography

[1] M. S. Dresselhaus, G. Dresselhaus and A. Jorio, Group Theory, Application to the Physics of Condensed Matter, Springer, Heidelberg (2008), ISBN-978-3-540-32897-1.

[2] M. Lazzeri and F. Mauri, Phys. Rev. Lett. **97**, 266407 (2006).

Appendix D

Dynamical corrections

Following the procedure Lazzeri et al. [1] and Pisana et al. [2] used in their work on graphene, self energy of phonon with wavevector q and frequency ω_ν is given by,

$$\sum(q, \omega_\nu + i\delta) = \frac{2}{N_k} \sum_{kij} \frac{|g^\nu_{ki,(k+q)j}|^2 (f_{ki} - f_{(k+q)j})}{\epsilon_{ki} - \epsilon_{(k+q)j} - (\hbar\omega_\nu + i\delta)}, \tag{D.1}$$

where k is the Blöch wave vector of the electronic state, N_k is the total number of k vectors, f_{ki} is the Fermi-Dirac distribution function and i, j denote band indices. $g_{ki,(k+q)j}$ is the matrix element of electron-phonon coupling between states ψ_{ki} & $\psi_{(k+q)j}$ and δ is a small real number. At $q = 0$ the real part of the $\sum$ gives the dynamical correction to phonon frequency $\hbar\Delta\omega$ [2]. In our analysis, we treat a single layer of Sb_2Se_3 and carry out integration over k in the Brillouin Zone in 2-D plane. For a phonon ν at Γ point and four-band Hamiltonian, [3]

$$\Delta\omega_{\Gamma_\nu} = Re[\sum(0,\omega_\nu)] = \frac{2A}{(2\pi)^2}\mathcal{P}\int_{-\infty}^{\infty} d^2k \sum_{i,j=1}^{4} \frac{|g^\nu_{ki,kj}|^2(f_{ki}-f_{kj})}{\epsilon_{ki}-\epsilon_{kj}-\hbar\omega_\nu} \qquad \text{(D.2)}$$

where $\mathcal{P}$ is the principle part of the integral.

Here, $g_{ki,kj}$ is given by $\langle ki|\, H_{A_{1g}}\, |kj\rangle$, $\langle ki|\, H_{A_{2u}}\, |kj\rangle$ and $\langle ki|\, H_{E_g}\, |kj\rangle$ respectively for A_{1g}, A_{2u} and E_g phonon modes. ki & kj are the eigenvectors of the effective four-band Hamiltonian $\mathcal{H}(\mathbf{k})$ as given by equation (1) by Zhang et al. [4] .

At the Γ point the effective four-band Hamiltonian is given by the following expression,

$$\mathcal{H}_\Gamma = \begin{bmatrix} C_0+M_0 & 0 & 0 & 0 \\ 0 & C_0-M_0 & 0 & 0 \\ 0 & 0 & C_0+M_0 & 0 \\ 0 & 0 & 0 & C_0-M_0 \end{bmatrix} \qquad \text{(D.3)}$$

To model the electronic structure across the electronic transition seen in the DFT calculations, we treat M_0 is function of pressure $M_0 = -k(P-P_c)$, where k is a positive number and P_c is the critical pressure.

The linewidth of a phonon mode in a crystal having strong electron phonon interaction is mainly determined by electron-phonon coupling (EPC) term in the Hamiltonian. The EPC contribution to FWHM (γ_ν) of a phonon

mode ν is given by the following expression [3],

$$\gamma_\nu = \frac{4\pi}{N_k} \sum_{k,i,j} |g^\nu_{ki,(k+q)j}|^2 (f_{ki} - f_{(k+q)j}) \times \delta(\epsilon_{ki} - \epsilon_{(k+q)j} + \hbar\omega_\nu), \qquad \text{(D.4)}$$

where δ is the Dirac delta function. Other terms in this expression have been explained in the previous sections.

Bibliography

[1] M. Lazzeri and F. Mauri, Phys. Rev. Lett. **97**, 266407 (2006).

[2] S. Pisana, M. Lazzeri, C. Casiraghi, K. S. Novoselov, A. K. Geim, A. C. Ferrari and F. Mauri, Nature Materials **6**, 198 (2007).

[3] M. Lazzeri, S. Piscanec, F. Mauri, A. C. Ferrari and J. Robertson, Phys. Rev. B **73**, 155426 (2006).

[4] H. Zhang, C. X. Liu, X. L. Qi, X. Dai, Z. Fang and S. C. Zhang, Nature Physics **5**, 438 (2009).

Appendix E

Dirac matrices

Dirac matrices or Dirac gamma matrices (Γ_n) are a class of 4×4 matrices which often arise in relativistic quantum mechanics through the Dirac equation in the description of 4-component spinor wave functions. These matrices are Hermitian and satisfy the following anti-commutating relation [1],

$$\frac{1}{2}(\Gamma_n\Gamma_m + \Gamma_m\Gamma_n) = \delta_{nm}I, \tag{E.1}$$

where δ is the Kronecker delta function and I is a 4×4 unity matrix. The five original matrices as given by Dirac are following [2],

$$\Gamma_1 = \begin{bmatrix} 0 & 0 & 0 & 1 \\ 0 & 0 & 1 & 0 \\ 0 & 1 & 0 & 0 \\ 1 & 0 & 0 & 0 \end{bmatrix} \qquad \Gamma_2 = \begin{bmatrix} 0 & 0 & 0 & -i \\ 0 & 0 & i & 0 \\ 0 & -i & 0 & 0 \\ i & 0 & 0 & 0 \end{bmatrix} \tag{E.2}$$

$$\Gamma_3 = \begin{bmatrix} 0 & 0 & 1 & 0 \\ 0 & 0 & 0 & -1 \\ 1 & 0 & 0 & 0 \\ 0 & -1 & 0 & 0 \end{bmatrix} \qquad \Gamma_4 = \begin{bmatrix} 1 & 0 & 0 & 0 \\ 0 & 1 & 0 & 0 \\ 0 & 0 & -1 & 0 \\ 0 & 0 & 0 & -1 \end{bmatrix} \tag{E.3}$$

$$\Gamma_5 = \begin{bmatrix} 0 & 0 & -i & 0 \\ 0 & 0 & 0 & -i \\ i & 0 & 0 & 0 \\ 0 & i & 0 & 0 \end{bmatrix} \tag{E.4}$$

Bibliography

[1] V. S. Mathur and S. Singh, Concepts in Quantum Mechanics, CRC Press, Boca Raton (2009), ISBN: 1420078720.

[2] G. B. Arfken and H. J. Weber, Mathematical Methods for Physicists, Academic Press, USA (2007), ISBN: 8131200809.